Development ePress. Posted online 27 February 2015
 | Development (2015) 142, 1-11 doi:10.1242/dev.116277

RESEARCH ARTICLE

# *Drosophila* MAGI interacts with RASSF8 to regulate E-Cadherin-based adherens junctions in the developing eye

**Sophie Zaessinger[1,2,3,4], Yanxiang Zhou[5], Sarah J. Bray[6], Nicolas Tapon[5] and Alexandre Djiane[1,2,3,4,*]**

## ABSTRACT

Morphogenesis is crucial during development to generate organs and tissues of the correct size and shape. During *Drosophila* late eye development, interommatidial cells (IOCs) rearrange to generate the highly organized pupal lattice, in which hexagonal ommatidial units pack tightly. This process involves the fine regulation of adherens junctions (AJs) and of adhesive E-Cadherin (E-Cad) complexes. Localized accumulation of Bazooka (Baz), the *Drosophila* PAR3 homolog, has emerged as a critical step to specify where new E-Cad complexes should be deposited during junction remodeling. However, the mechanisms controlling the correct localization of Baz are still only partly understood. We show here that *Drosophila* Magi, the sole fly homolog of the mammalian MAGI scaffolds, is an upstream regulator of E-Cad-based AJs during cell rearrangements, and that *Magi* mutant IOCs fail to reach their correct position. We uncover a direct physical interaction between Magi and the Ras association domain protein RASSF8 through a WW domain-PPxY motif binding, and show that apical Magi recruits the RASSF8-ASPP complex during AJ remodeling in IOCs. We further show that this Magi complex is required for the cortical recruitment of Baz and of the E-Cad-associated proteins α- and β-catenin. We propose that, by controlling the proper localization of Baz to remodeling junctions, Magi and the RASSF8-ASPP complex promote the recruitment or stabilization of E-Cad complexes at junction sites.

**KEY WORDS: Adherens junctions, MAGI scaffolds, Morphogenesis**

## INTRODUCTION

During development, tissues undergo morphogenesis to adopt their specific sizes and shapes, a process driven by the behaviors of individual cells (Heisenberg and Bellaïche, 2013). For instance, the stereotypical arrangement of hexagonal ommatidia in the *Drosophila* adult compound eye is achieved during earlier pupal stages through cell rearrangements. Each ommatidium is composed of eight photoreceptors beneath four cone cells, and is surrounded by two primary pigment cells (Bao et al., 2010). Ommatidia are separated by secondary and tertiary pigment cells [interommatidial cells (IOCs)] arranged in a repetitive hexagonal lattice. Initially, an excess of unpatterned interommatidial precursor cells (IPCs) lies between the ommatidia. Between 18 h and 42 h after puparium formation (APF), the unpatterned IPCs first rearrange into a single row between neighboring ommatidia and the excess are removed by apoptosis, giving rise to the stereotypical repetitive hexagonal units of the *Drosophila* eye (Cagan, 2009).

Regulated cell-cell adhesion is crucial for correct formation of the interommatidial lattice. For example, IPC rearrangement requires the careful modulation of adherens junctions (AJs) (Tepass and Harris, 2007). This remodeling of AJs involves the destruction of old E-Cadherin (E-Cad)-based contacts and the creation of new ones (E-Cad is also known as Shotgun – FlyBase). Studies in *Drosophila* embryos and pupae have highlighted crucial roles for Bazooka (Baz), the *Drosophila* PAR3 homolog, in specifying *de novo* E-Cad deposition during remodeling (Desai et al., 2013; McGill et al., 2009; McKinley et al., 2012; Walther and Pichaud, 2010) and for the actin cytoskeleton in controlling the dynamics of individual junctions (Levayer et al., 2011; Rauzi et al., 2010). In the *Drosophila* pupal eye, IOC rearrangements and hence junction remodeling are also regulated by heterophilic interactions between Irre family adhesion molecules, such as Hibris and Roughest [homologs of vertebrate Nephrin (NPHS1) and NEPH1 (KIRREL), respectively] (Bao and Cagan, 2005; Bao et al., 2010; Reiter et al., 1996). Loss of any of these adhesion molecules leads to defects in IOC rearrangement as well as in apoptosis, suggesting that IOC rearrangement is necessary for apoptosis.

Recently, the N-terminal Ras association (RA) domain-containing protein RASSF8 (Ras association domain family 8) was shown to regulate *Drosophila* pupal eye morphogenesis and the AJ integrity of IOCs (Langton et al., 2009). In *Drosophila* epithelial cells, RASSF8 is localized apically and binds to ASPP (Ankyrin-repeat, SH3-domain, and proline-rich-region containing protein), the fly homolog of the p53 activating partners ASPP1 (PPP1R13B) and ASPP2 (TRP53BP2). The RASSF8-ASPP complex regulates the activity of Src kinases, which promote AJ remodeling (Langton et al., 2007, 2009; Vidal et al., 2006). How this complex interacts with other key players of AJ regulation to control AJ remodeling during eye morphogenesis remains unexplored.

MAGI (membrane-associated guanylate kinase inverted) proteins are molecular scaffolds with several protein-protein interaction (WW and PDZ) domains. MAGI proteins localize at apical junctions and bind β-catenin as well as other apical proteins (Dobrosotskaya and James, 2000; Ide et al., 1999; Kawajiri et al., 2000). For example, MAGI1 binds and activates the guanine nucleotide exchange factor for the junction remodeling small GTPase RAP1, which in turn regulates maturation of the AJs (Sakurai et al., 2006). MAGIs also bind to and stabilize the tumor suppressor PTEN (phosphatase and tensin homolog) at the membrane, leading to increased PTEN activity (Kotelevets et al., 2005; Subauste et al., 2005; Wu et al., 2000a,b; Zmajkovicova et al., 2013). Taken together, these studies suggest that MAGIs may modulate epithelial cell adhesion and, through PTEN, restrict proliferation. *MAGI2* and *MAGI3* mutations have been identified in prostate, colorectal and breast cancer genomes (Banerji et al., 2012;

[1]IRCM, Institut de Recherche en Cancérologie de Montpellier, Montpellier F-34298, France. [2]INSERM, U1194, Montpellier F-34298, France. [3]Université de Montpellier, Montpellier F-34090, France. [4]Institut régional du Cancer de Montpellier, Montpellier F-34298, France. [5]Apoptosis and Proliferation Control Laboratory, Cancer Research UK, London Research Institute, 44 Lincoln's Inn Fields, London WC2A 3LY, UK. [6]Department of Physiology Development and Neuroscience, University of Cambridge, Downing Street, Cambridge CB2 3DY, UK.

*Author for correspondence (alexandre.djiane@inserm.fr)

**Received 4 August 2014; Accepted 19 January 2015**

Development (2015) 142, 1-11 doi:10.1242/dev.116277

Berger et al., 2011; Pleasance et al., 2010), suggesting that MAGI proteins might be involved in cancers.

Here, we investigate the function of *Drosophila Magi*, the sole fly homolog of the three human MAGI genes, and demonstrate that it regulates AJ dynamics and IOC number. In *Magi* mutants, IOCs of the pupal lattice fail to rearrange, resulting in eyes with mislocalized supernumerary cells. We have identified RASSF8 as a Magi binding partner and show that these proteins interact physically and functionally during pupal eye development. Magi localizes at the AJs in *Drosophila* pupal eye epithelial cells, where it recruits the RASSF8-ASPP complex. During IOC rearrangement, Magi is required for E-Cad-based junction integrity, a function dependent on its WW domains and on its interaction with RASSF8. We show that Magi, RASSF8 and ASPP are required for the recruitment of Baz at the membrane. We propose that, by recruiting the RASSF8-ASPP complex at the AJs during remodeling in *Drosophila* eye IOCs, Magi helps specify domains of the membrane where Baz promotes the accumulation of E-Cad to generate new junctions.

## RESULTS

### *Magi* controls cell numbers in the *Drosophila* pupal eye

To study *Magi* function in *Drosophila* we generated mutations by mobilizing a transposon (P element *P{GSV6}GS6093*) located just upstream of the *Magi* locus, between *Magi* and *CG9406*. Among the local genomic deletions generated by the imprecise excision of this transposon, excision ex214 affected only *Magi*. Genomic PCR mapped the deficiency to the first three exons of *Magi*, deleting the transcription start site, the initiating methionine, and the first half of the first WW domain. The rest of the *Magi* gene and the neighboring genes *mago*, *CG9406* and *Xbp1* are unaffected (supplementary material Fig. S1A and Fig. S2A). In $Magi^{ex214}$ mutant cells, no Magi protein expression could be detected using a polyclonal anti-Magi antibody that we generated directed against the PDZ3 and 4 domains (supplementary material Fig. S1B). Finally, western blot analysis using the anti-Magi antibody revealed the absence of a band at the expected size for the protein (~130 kDa) in $Magi^{ex214}$ mutants and did not reveal any shorter products (supplementary material Fig. S1C), suggesting that no truncated protein is expressed. Together, these results suggest that $Magi^{ex214}$ is a molecular null allele.

$Magi^{ex214}$ homozygous flies are viable and fertile, but exhibit slightly enlarged wings (supplementary material Table S1) and mildly rough eyes (Fig. 1B,B′). The latter arises because the ommatidia are not surrounded by the proper numbers of neighbors and interommatidial bristles (six and three, respectively, in wild type) resulting in packing defects (Fig. 1D). In *Magi* mutants, ~13% of ommatidia have abnormal numbers of neighbors compared with 0.4% in wild-type controls (Fig. 1D). Similarly, ~35% of *Magi* mutant ommatidia have abnormal numbers of interommatidial bristles compared with 9.5% in wild type (Fig. 1E). This phenotype is not enhanced when $Magi^{ex214}$ is transheterozygous with a mapped deficiency that uncovers the *Magi* locus [*Df(2R)Exel6072*], arguing that $Magi^{ex214}$ behaves as a genetic null mutation. The rough eye phenotype and cell packing defects are completely rescued by low-level ubiquitous expression of full-length *Magi* [using the *ubiquitin* promoter, which drives expression of *Magi* transgenes at levels similar to (~1.5-fold) the endogenous protein; supplementary material Fig. S1D,E], proving that the defects observed are specific to the *Magi* mutation (Fig. 1C-E).

The mild rough eye in $Magi^{ex214}$ can be explained by the presence of additional mislocalized IOCs as well as extra interommatidial bristles in pupal retinas (Fig. 1A″,B″). There were on average 12.25±1.00 IOCs per ommatidium in the *Magi* mutant, as compared with 9.04±0.06 in wild type (see supplementary Materials and Methods for quantification procedures; Fig. 1F). $Magi^{ex214}$ pupal eyes also exhibited sorting defects, whereby secondary pigment

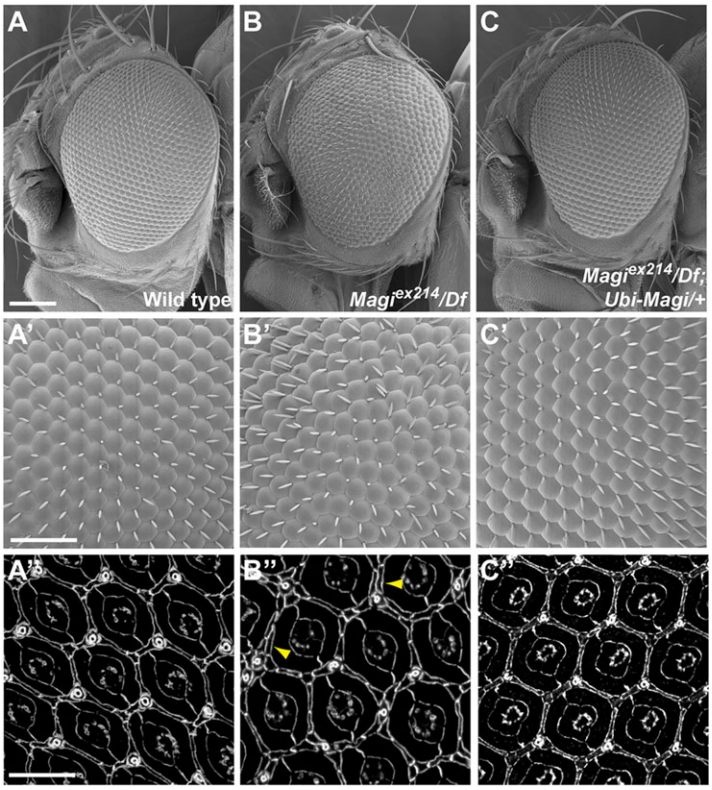


**Fig. 1. Magi controls morphogenesis of the *Drosophila* pupal eye lattice.** (A-C) Scanning electron micrographs showing the effect of *Magi* mutation on the external architecture of the adult eye. *Magi* mutant adults have a mild rough eye phenotype (B) compared with wild type (A), which is rescued by providing a ubiquitously expressed *Magi* transgene (C). (A′-C′) High magnification of the adult compound eye corresponding to A-C. The regular hexagonal packing of ommatidial units of the wild type (A′) is affected in *Magi* mutants (B′) and rescued by providing wild-type *Magi* (C′). (A″-C″) Pupal eye at 44 h APF stained for E-Cad, showing the ommatidial organization corresponding to A-C. *Magi* mutant eyes have extra IOCs (B″, arrowheads) compared with wild-type controls (A″). Total rescue is seen when a wild-type *Magi* transgene is provided (C″). (D,E) Quantification of the effects observed in A′-C′. The total number of ommatidia scored ranged from 433 to 541 depending on genotype. (F) Quantification of the number of IOCs per ommatidium (see Materials and Methods). (D-F) Error bars indicate s.e.m.; ***$P$<0.001, **$P$<0.01, n.s., not significant (unpaired $t$-test). Scale bars: 100 µm in A; 50 µm in A′; 10 µm in A″.

Development (2015) 142, 1-11 doi:10.1242/dev.116277

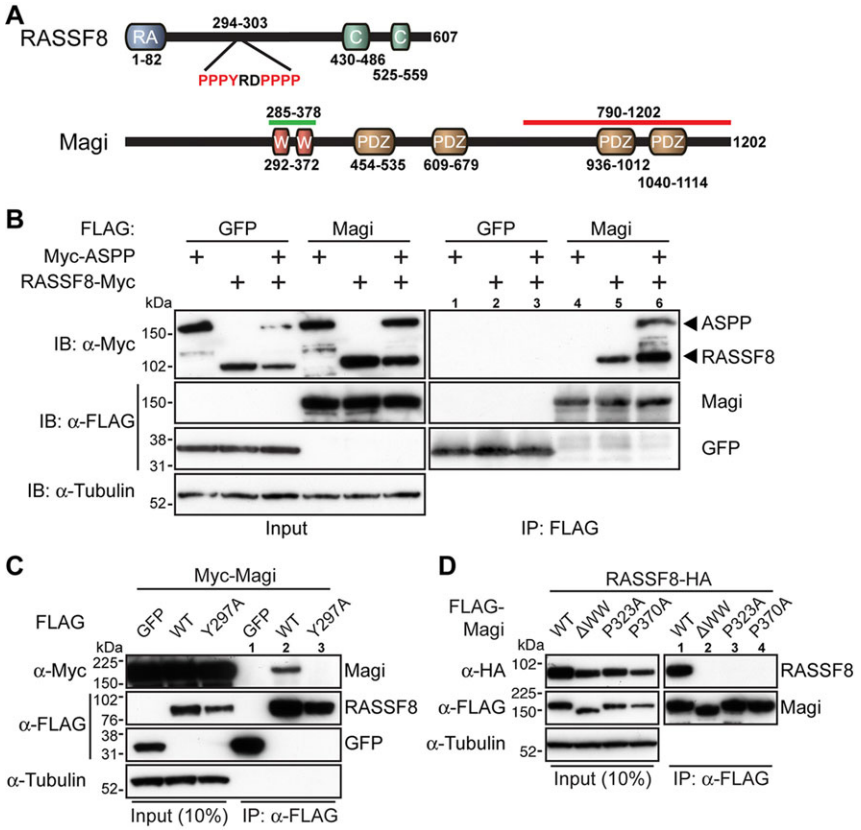


**Fig. 2. Magi binds to RASSF8.** (A) Schematics of *Drosophila* RASSF8 and Magi structure. Highlighted are the RASSF8 residues 294-303 with a PPxY motif, the Magi residues 285-378 (green line) representing the common fragment of the Magi clones identified by two-hybrid analysis using RASSF8 as bait, and the Magi residues 790-1202 (red line) representing the fragment used to raise the anti-Magi antibody. The PDZ (PSD95/Dlg1/Zo1), WW, Ras association (RA) and coiled-coil (C) domains are shown. (B) RASSF8 co-immunoprecipitates with Magi. (Left) Western blot of cleared lysates from cells expressing either FLAG-tagged GFP (FLAG-GFP, negative control) or FLAG-Magi with Myc-ASPP or Myc-RASSF8, or both. (Right) Western blot following immunoprecipitation with anti-FLAG. Myc-RASSF8 co-immunoprecipitates only with FLAG-Magi (lanes 5 and 6) and not with FLAG-GFP (lanes 2 and 3). Myc-ASPP co-immunoprecipitates with FLAG-Magi only in the presence of RASSF8 (lane 6). (C) The PPxY motif in RASSF8 is required for the interaction with Magi. (Left) Western blot of cleared lysates from cells expressing Myc-Magi with either FLAG-GFP (negative control) or FLAG-RASSF8 (WT), or FLAG-RASSF8$^{Y297A}$ in which Y297 is substituted for alanine (Y297A). (Right) Western blot following immunoprecipitation with anti-FLAG. Myc-Magi co-immunoprecipitates only with FLAG-RASSF8 (lane 2) and not with FLAG-GFP (lane 1) or FLAG-RASSF8$^{Y297A}$ (lane 3). (D) The WW domains in Magi are required for the interaction with RASSF8. (Left) Western blot of cleared lysates from cells expressing HA-RASSF8 with different FLAG-Magi mutant constructs: wild-type Magi (WT), Magi deleted of the two WW domains (ΔWW), Magi in which P232 in the first WW is mutated (P232A), and Magi in which P370 in the second WW is mutated (P370A). (Right) Western blot following immunoprecipitation with anti-FLAG. HA-RASSF8 co-immunoprecipitates only with HA-Magi (WT, lane 1) and not with MagiΔWW (ΔWW, lane 2) or Magi with point mutations in the WW domains (lanes 3 and 4).

cells contacted other secondary pigment cells instead of being surrounded by primary pigment cells (Fig. 1B″, arrowheads). The number of photoreceptors, cone cells and primary pigment cells was unaffected. These defects in IOC numbers and sorting were completely rescued by a wild-type *Magi* transgene (average of 8.97±0.14 IOCs per ommatidium; Fig. 1C″,F). Conversely, overexpression of Magi in all pupal eye cells (using *GMR-Gal4*) led to a loss of IOCs (average of 7.40±0.65 IOCs per ommatidium; supplementary material Fig. S2B, arrowheads), leading to packing defects and an externally rough eye (see Fig. 3K). These results show that *Magi* is required for the control of IOC number and for the proper sorting of IOCs during *Drosophila* pupal eye development.

We then tested whether the extra IOCs in *Magi* mutants could be due to a defect in the developmental apoptosis of IOCs occurring between 18 and 42 h APF (Cagan, 2009). Assessing the number of apoptotic cells in wild-type and *Magi* mutant tissues within the same retinas, we did not detect any significant difference (6.12±2.20 and 5.64±1.89 apoptotic cells per arbitrary surface unit, respectively; $P$=0.395, paired $t$-test; supplementary material Fig. S2C,D). We note, however, that the small number of extra IOCs in *Magi* mutants suggests that *Magi* would only affect a small proportion of the cells undergoing developmental apoptosis in the pupal eye, making it difficult to distinguish the Magi-regulated effects from the bulk of apoptotic events.

### RASSF8 is a binding partner of Magi

To elucidate Magi function during eye development, we sought to identify its molecular partners. One candidate was ASPP, as *ASPP* loss-of-function alleles cause similar phenotypes to *Magi* mutations in the developing *Drosophila* eye (Langton et al., 2007), and because human ASPP2 binds to human MAGI1 (Pirozzi et al., 1997). Furthermore, several clones of *Drosophila Magi* were isolated in a yeast two-hybrid screen using RASSF8, a partner of ASPP, as bait. RASSF8 is a strong binding partner of ASPP, and *RASSF8* mutant pupal eyes exhibit a phenotype similar to that of *Magi* mutants (Langton et al., 2009). We therefore first tested the Magi-RASSF8 interaction by co-immunoprecipitation (co-IP), and confirmed that Myc-tagged RASSF8 could be co-purified with FLAG-tagged Magi (Fig. 2B). Although ASPP alone did not co-immunoprecipitate with Magi, when ASPP was co-expressed

Development (2015) 142, 1-11 doi:10.1242/dev.116277

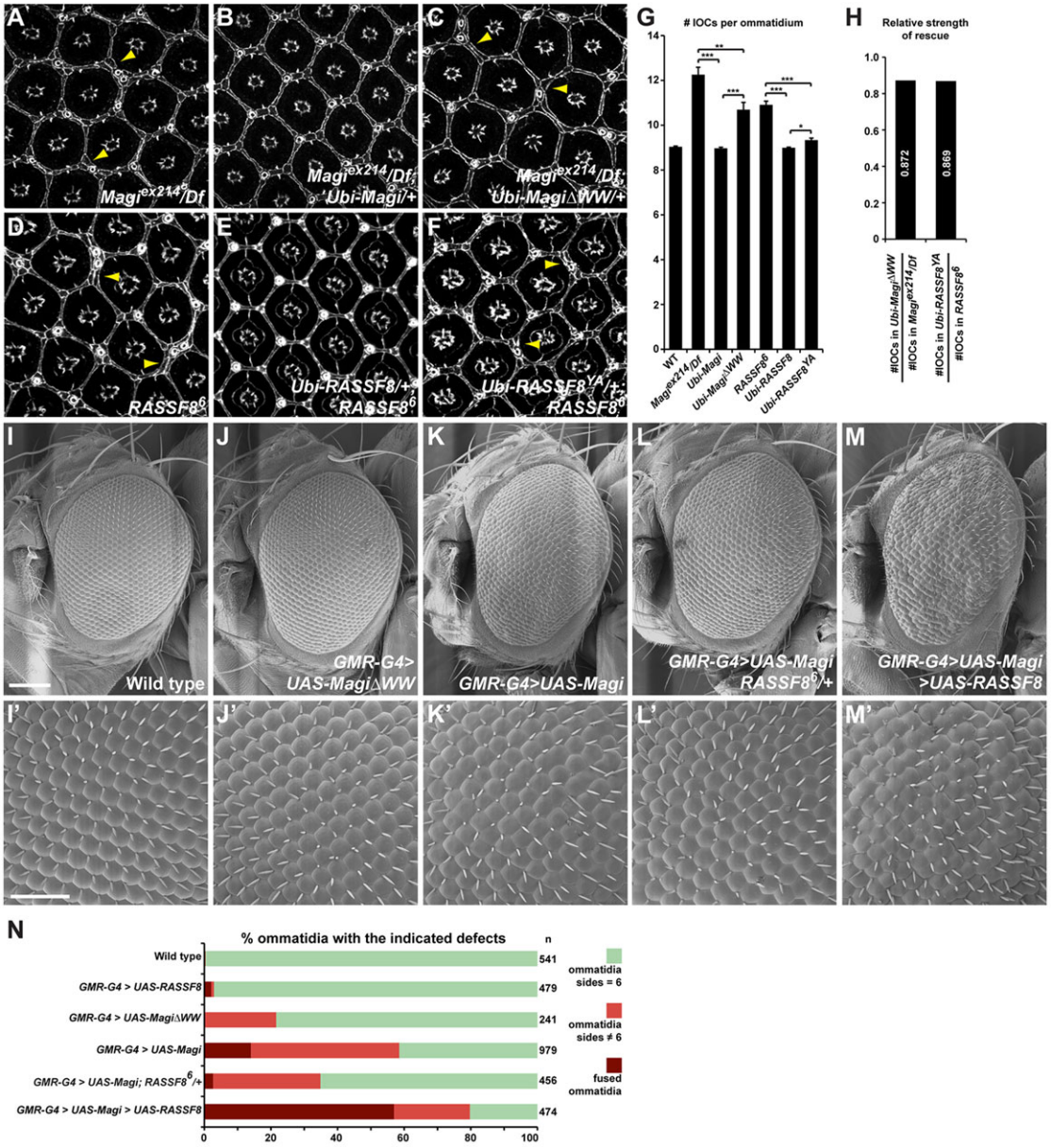


**Fig. 3. *Magi* acts through *RASSF8*.** (A-F) Pupal eye at 44 h APF stained for E-Cad showing ommatidial organization. Arrowheads highlight extra IOCs compared with wild type. Whereas the supernumerary IOC phenotype in *Magi* mutants (A) is completely rescued by introducing a wild-type *Magi* transgene (B), only partial rescue is seen with a *MagiΔWW* transgene (C). Similarly, only a wild-type *RASSF8* transgene (E), and not a *RASSF8*$^{YA}$ transgene mutated in its Magi-interacting motif (F), is able to fully rescue the extra IOC phenotype in *RASSF8* mutants (D). (G) Quantification of the number of IOCs per ommatidium in A-F (see Materials and Methods). s.e.m. is shown; ***$P$<0.001, **$P$<0.01, *$P$<0.05 (unpaired $t$-test). (H) Strength of rescue obtained after normalization. Normalization was obtained by dividing the number of IOCs in the different rescue experiments by the number of IOCs in the corresponding *Magi* or *RASSF8* mutant background. (I-M) Scanning electron microscopy of *Drosophila* adult eyes following *GMR-Gal4*-driven overexpression. Full-length Magi overexpression produces a mild rough eye (K) compared with wild type (I), while MagiΔWW has a weaker effect (J) (all transgenes are inserted at the same locus ensuring equivalent expression levels). This effect of Magi is strongly suppressed by removing one copy of *RASSF8* (*RASSF8*$^{6}$/+; L) but is enhanced by co-expressing *RASSF8* (M). (I′-M′) High magnification of adult eyes corresponding to I-M. Note the almost wild-type packing after *MagiΔWW* (J′) overexpression, and the very disorganized eye structure after *Magi* and *RASSF8* co-overexpression (M′). (N) Quantification of the effects observed in I′-M′, highlighting the suppression of the effects of Magi overexpression by *RASSF8* mutants. *n*, total number of ommatidia scored per genotype. Scale bars: 100 µm in I; 50 µm in I′.

with RASSF8 both proteins co-purified with FLAG-Magi (Fig. 2B). This suggests that ASPP might not interact directly with Magi in *Drosophila*, but forms a ternary complex through RASSF8.

The Magi fragments isolated in the two-hybrid screen with RASSF8 spanned the two WW domains of Magi (Fig. 2A; supplementary material Table S2). Since RASSF8 contains a PPxY motif, which is a known ligand for WW domains, we tested whether Magi could be interacting, via its WW domains, with RASSF8 through this motif. We generated a mutant RASSF8 protein in which tyrosine residue 297 of the PPxY motif was mutated to an alanine. This RASSF8$^{Y297A}$ mutant could no longer interact with Magi in co-IP experiments (Fig. 2C). To confirm that RASSF8 binds to the WW domains of Magi we generated three different mutant versions by (1) deleting the two WW domains (ΔWW), (2) substituting proline 323 in the first WW domain with an alanine (P323A), and (3) substituting proline 370 in the second WW

Development (2015) 142, 1-11 doi:10.1242/dev.116277

domain with an alanine (P370A). In co-IP experiments, only the wild-type form of Magi pulled down RASSF8 (Fig. 2D). Mutating either WW domain was sufficient to abrogate the binding. These results show that binding of RASSF8 and Magi is mediated by a PPxY motif-WW domain interaction.

### The physical interaction between RASSF8 and Magi is required for their full function

As Magi and RASSF8 form a complex, we investigated the consequences of disrupting the Magi-RASSF8 physical interaction on their activities.

Whereas the ubiquitous expression of full-length Magi fully rescued the adult external rough eye phenotype and packing defects of the *Magi* mutant (Fig. 1C-F), a mutant form of Magi lacking the WW RASSF8-interacting domains gave only a partial rescue (2% of ommatidia with the improper number of neighbors and 23% with bristle abnormalities). Furthermore, whereas the extra IOC phenotype in *Magi* mutants (12.25±1.00 IOCs per ommatidium compared with 9.04±0.06 in wild type, a 36% increase) was completely rescued by wild-type Magi (Fig. 3B,G), it was only partially rescued by MagiΔWW (10.69±0.92 IOCs per ommatidium, an 18% increase; Fig. 3C,G). The MagiΔWW mutant is expressed at very similar levels to wild-type Magi and ∼1.5-fold more than endogenous Magi, showing that the weaker effects of MagiΔWW are not due to reduced protein levels (supplementary material Fig. S1D,E). This demonstrates that the WW domains of Magi are required for full function.

Similarly, the extra IOC phenotype observed in *RASSF8* mutants (10.91±0.36, a 21% increase compared with wild type) was completely rescued by expression of a wild-type form of RASSF8 (Fig. 3E,G), but only partially rescued by expression of the RASSF8$^{Y297A}$ variant in which the Magi-binding PPxY motif was mutated (9.48±0.28, a 5% increase; Fig. 3F,G). We note that when normalized to the extra IOC phenotype observed in the *Magi* and *RASSF8* mutants, the extents of rescue by MagiΔWW and RASSF8$^{Y297A}$ were similar (0.872 and 0.869, respectively; Fig. 3H). Together, these results strongly suggest that the physical interaction between Magi and RASSF8 is required for their functions in controlling IOC numbers and their rearrangement.

### RASSF8 mediates the effects of Magi in the *Drosophila* eye

To further establish the relevance of RASSF8 for Magi function, we tested the functional requirements for RASSF8 under conditions in which Magi overexpression elicits ommatidial packing defects. As expected, MagiΔWW lacking the RASSF8-interacting WW domains gave a far milder phenotype than wild-type Magi when overexpressed (Fig. 3J,K,N), suggesting that the Magi-RASSF8 interaction is important for the effects of excess Magi.

Furthermore, the rough eye phenotype induced by Magi overexpression (Fig. 3K) was efficiently suppressed by removing one copy of *RASSF8* and was strongly enhanced by co-expressing RASSF8 (Fig. 3L-N; note that overexpressed RASSF8 alone had no effect, Fig. 3N). In eyes with overexpressed Magi, 58.5% of ommatidia had defects. The proportion of defective ommatidia was reduced to 34.9% in a *RASSF8* heterozygous background, but increased to 79.7% when RASSF8 was co-expressed (Fig. 3N). These results argue that RASSF8 mediates the effect of Magi (see also supplementary material Table S3) and, taken with the other data, suggest that the control of IOC numbers, cell rearrangements and packing during *Drosophila* pupal eye development requires a complex containing Magi and RASSF8.

### Magi recruits RASSF8 and ASPP at AJs in the pupal eye

The RASSF8-ASPP complex is localized at AJs and has been proposed to regulate AJ remodeling that occurs in the eye around 24 h APF (Langton et al., 2007, 2009). Similar to RASSF8, in wing imaginal discs (Fig. 4A and supplementary material Fig. S1B) and in 24-h APF pupal eye discs (Fig. 4D) Magi colocalized with E-Cad at AJs (Fig. 4A,D). Its position was restricted to the AJ: apical to the septate junction protein Discs large (Dlg) (Fig. 4B) and basal to the subapical marker aPKC (Fig. 4A).

The physical interaction between Magi and RASSF8 raises the possibility that they could reciprocally regulate their localization at AJs. However, Magi localization at the AJ was found to be independent of both RASSF8 and ASPP. Focusing on the particular timing when RASSF8 and ASPP are required for AJ remodeling, both wild-type Magi and a mutant form lacking the WW domains localized correctly at AJs (expressed using *ubiquitin* promoter; Fig. 5A,B), even in the absence of endogenous Magi (*Magi* null mutant background). We obtained similar results in larval wing discs, where GFP-tagged wild-type and WW-deficient forms of Magi both localized at the AJs (expressed using *patched-Gal4*; Fig. 4B,C). These results show that the RASSF8-interacting WW domains are dispensable for Magi localization at AJs. Furthermore, the localization of Magi was unaffected in either *RASSF8* or *ASPP* mutant cells, whether in wing imaginal discs (supplementary material Fig. S3A,B,E,F) or in 24-h APF eye discs (Fig. 5C,D). Finally, even in the absence of both *RASSF8* and *ASPP*, Magi was still properly localized at the membrane of IOCs at 24 h APF (Fig. 5E), ruling out any potential redundancy between RASSF8 and ASPP. Taken together, these results show

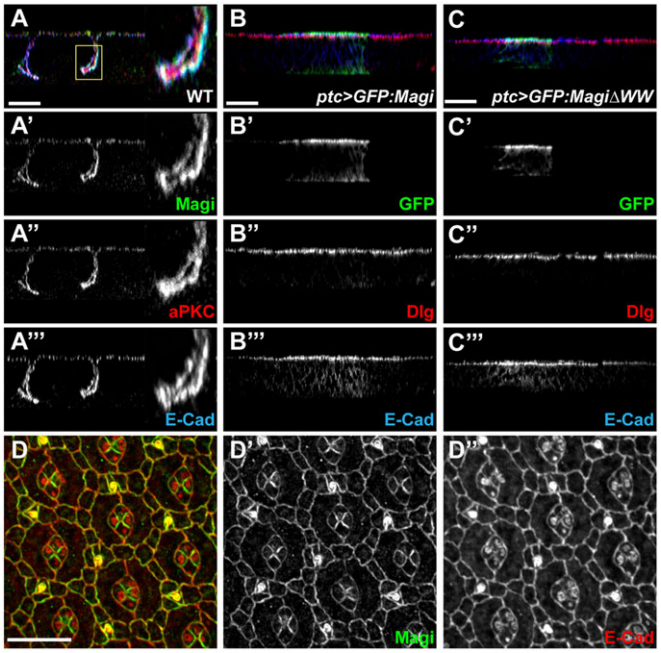


**Fig. 4. Magi AJ localization is independent of RASSF8 and ASPP.** (A-A‴) In larval wing imaginal disc epithelial cells Magi (green, A′) colocalizes with E-Cad (blue, A‴) at the AJ level, basal to aPKC (red, A″). A confocal *z*-section is shown. The boxed region is shown at higher magnification to the right. (B-C‴) Confocal *z*-sections of larval wing discs overexpressing GFP-tagged Magi (B) or MagiΔWW (C) using the *ptc-Gal4* driver. Both Magi constructs (GFP, green, B′,C′) colocalize with E-Cad (blue, B‴,C‴), apical to the septate junction protein Dlg (red, B″,C″). (D-D″) In 24-h APF pupal eye discs, Magi (green, D′) is localized at cell junctions in IOCs together with E-Cad (red, D″). Scale bars: 20 µm in A-C; 10 µm in D.

Development (2015) 142, 1-11 doi:10.1242/dev.116277

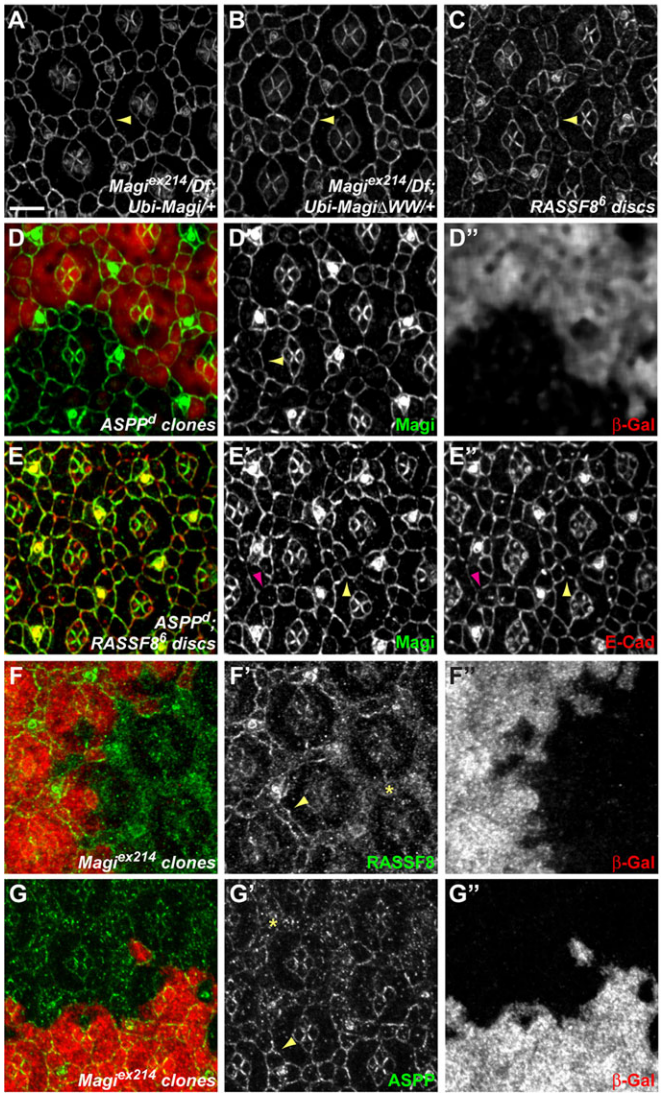


**Fig. 5. Magi recruits RASSF8 and ASPP.** (A-C) 24-h APF pupal eye discs stained for Magi. Arrowheads mark membrane recruitment of Magi. In *Magi* null mutant discs, both Magi (A) and MagiΔWW (B) are recruited at the membrane. Similarly, in a *RASSF8* whole mutant disc, Magi is correctly localized at junctions (C). (D-D″) At 24-h APF, in *ASPP* mutant clones marked by the absence of β-galactosidase (red, D″), Magi (green, D′) protein levels and apical localization are unaffected (arrowhead). (E-E″) At 24 h APF, in *ASPP; RASSF8* double-mutant discs, Magi (green, E′) is properly localized at the cortex, even though a few gaps can be seen. There are many more gaps for E-Cad (red, E″), which overlap (purple arrowhead) or not (yellow arrowhead) with the Magi gaps. (F-G″) 24-h APF *Magi* mutant clones marked by the absence of β-galactosidase (red, F″,G″). RASSF8 (F, green; F′) and ASPP (G, green; G′) are mislocalized (asterisk) in *Magi* mutant IOCs compared with their membrane localization in wild-type tissues (arrowheads). Scale bar: 5 µm.

that Magi localizes at AJs independently of either RASSF8 or ASPP.

By contrast, RASSF8 and ASPP localization at AJs in pupal eye discs was dependent on Magi. In *Magi* mutant clones at 24 h APF both RASSF8 and ASPP were absent from the membrane and accumulated in the cytoplasm of IOCs (Fig. 5F,G). We note, however, that a residual amount of ASPP was still cortical in *Magi* mutant clones (Fig. 5G). This suggests the existence of an *in vivo* ternary molecular complex between Magi and RASSF8-ASPP and validates in pupal IOCs the direct physical interaction detected between Magi and RASSF8. However, RASSF8 and ASPP were not dependent on Magi for their AJ localization in larval wing disc epithelial cells (supplementary material Fig. S3C,D,G,H). This suggests that either the interaction between Magi and the RASSF8-ASPP complex is context dependent or that, at least in the larval disc, redundant localization mechanisms to Magi exist.

### Magi affects AJ integrity in the pupal eye similarly to RASSF8 and ASPP

As ASPP and RASSF8 are required for AJ integrity and IPC rearrangement, we examined these processes in *Magi* mutants. During the formation of the interommatidial lattice, IPCs undergo extensive rearrangements. This process requires the redistribution of AJs (Tepass and Harris, 2007) and fails in the *RASSF8* or *ASPP* mutants, leading to interrupted AJs at 24 h APF (Langton et al., 2007, 2009). We therefore investigated the morphology of AJs in *Magi* mutant cells, and observed interruptions in the E-Cad belt at 24 h APF (Fig. 6A). Whereas we could detect on average 0.25±0.10 interruptions in the cortical E-Cad staining per IOC in wild-type clones, this increased to 0.73±0.27 in neighboring *Magi* mutant clones (Fig. 6B). Using the same quantification method, we could detect 1.49±0.32 E-Cad gaps per IOC in *ASPP* mutants, confirming the similarity in the early E-Cad disruption phenotypes.

Given the effect of Magi on E-Cad localization during AJ remodeling, we tested whether Magi could also affect α- and β-catenins, which are core components of Cadherin-based junctions. Strikingly, in *Magi* mutant clones at 24 h APF, the membrane levels of both α-catenin and β-catenin [Armadillo (Arm) – FlyBase] were reduced compared with neighboring wild-type cells (Fig. 6C,E,F,H). This was accompanied by an increase in intracellular puncta containing these proteins. Within *Magi* mutant clones, there were 6.76±1.58 α-catenin and 5.88±0.64 β-catenin intracellular puncta per IOC, as compared with wild-type cells which had 3.01±0.84 and 3.66±0.93 puncta, respectively (Fig. 6D,G). Taken together, these results suggest that during remodeling *Magi* mutant cells form abnormal AJs with less localized E-Cad and catenin proteins. Halving the dosage of β-catenin strongly enhances the E-Cad interruptions in IOCs seen in *Magi* mutants at 24 h APF (supplementary material Fig. S4A,B), suggesting that Magi could be acting redundantly with other β-catenin-localizing mechanisms to regulate E-Cad-based AJs.

We note, however, that such interruptions to AJ structure in *Magi* mutants occur transiently at the time of IOC sorting, and are not evident at later stages (pupal retina lattice at 44 h APF; Fig. 1B″) or in the larval wing disc epithelia. Magi function might therefore only be crucial in tissues undergoing rapid cell rearrangements.

### Magi controls Baz localization during IOC remodeling

The apical scaffold protein Baz/PAR3 has been implicated in AJ stability and remodeling in several developmental processes (Desai et al., 2013; McGill et al., 2009; McKinley et al., 2012; Walther and Pichaud, 2010). It has been proposed to promote the coalescence of small cadherin-catenin clusters to form nascent junctions during cellularization in the embryo (McGill et al., 2009; McKinley et al., 2012), a process mediated at least in part through the binding and recruitment of β-catenin (Wei et al., 2005). Since E-Cad-based junctions and catenin membrane distributions were disrupted in *Magi* mutant cells, we tested whether Baz could also be affected. Strikingly, Baz was lost from the membrane of IOCs in *Magi* mutant clones at 24 h APF, and accumulated in the cytoplasm (Fig. 7A). Baz localization was however normal in *Magi* mutant cells by 44 h APF (supplementary material Fig. S4C).

Development (2015) 142, 1-11 doi:10.1242/dev.116277

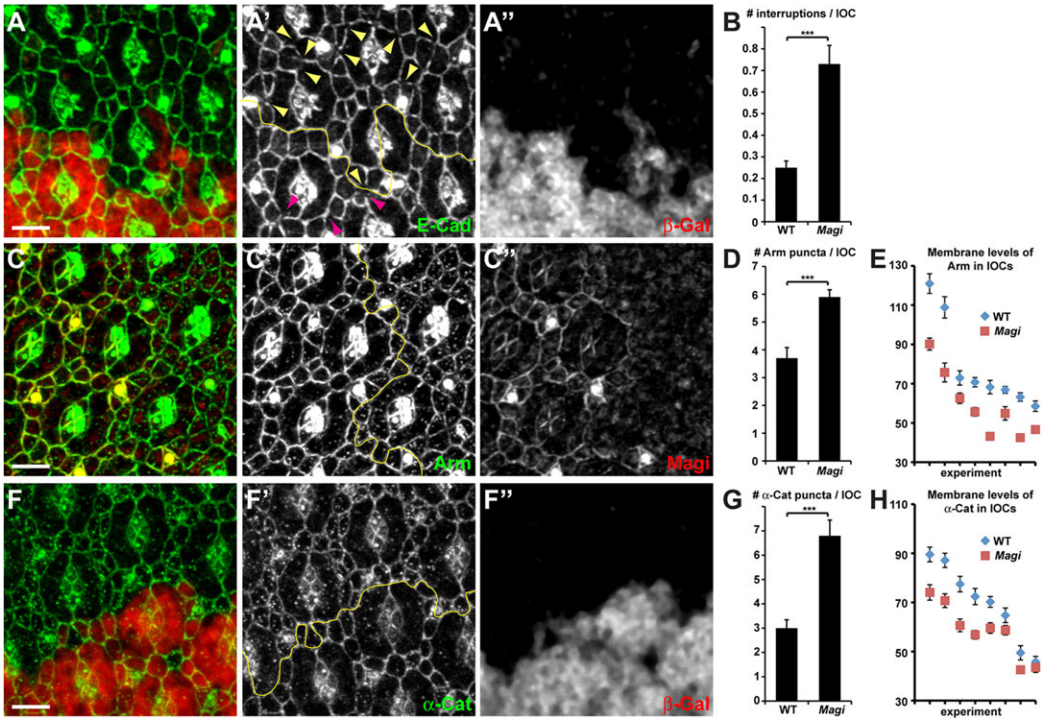


**Fig. 6. *Magi* mutant has abnormal AJs.** (A-A″,C-C″,F-F″) 24-h APF pupal eye discs with *Magi* mutant clones marked by the absence of β-galactosidase (red, A″,F″) or the absence of Magi (red, C″). Yellow lines (A′,C′,F′) mark the boundaries between wild-type and mutant tissues. (A) In *Magi* mutant tissue, E-Cad staining (green, A′) is frequently interrupted (yellow arrowheads) compared with wild type (purple arrowheads). (C,F) In *Magi* mutant tissue, β-catenin (Arm; green, C′) and α-catenin (α-Cat; green, F′) are less cortical and accumulate in cytoplasmic vesicles in IOCs. (B,D,G) Quantification of E-Cad interruptions (B), Arm vesicles (D) and α-Cat vesicles (G) in wild-type and *Magi* mutant tissues corresponding to A, C and F, respectively. s.e.m. is shown; ***$P$<0.001 (unpaired *t*-test). (E,H) Quantification of Arm (E) and α-Cat (H) membrane levels between IOCs in wild-type and *Magi* mutant tissues corresponding to C and F, respectively. Eight independent pairs of wild-type and *Magi* mutant tissues are shown and plotted by decreasing arbitrary average pixel intensity. Levels in wild type are always higher than those in *Magi*. s.e.m. is shown; $P$<0.001 (paired *t*-test). Scale bars: 5 µm.

We then investigated whether the interaction between Magi and the RASSF8-ASPP complex was required for Baz membrane recruitment. First, we confirmed that the effects were completely rescued by expression of wild-type Magi. By contrast, Baz localization to the membrane was still defective in the presence of MagiΔWW (Fig. 7B-D). This suggests that the binding of Magi to RASSF8 is required for Baz membrane localization in IOCs at 24 h APF. In agreement, Baz was also mislocalized in *RASSF8* and *ASPP* mutant cells, albeit to a lesser extent than in *Magi* mutants (Fig. 7E,F). Thus, Magi, and its interaction with the RASSF8-ASPP complex, is required for normal Baz localization at AJs in IOCs at 24 h APF during tissue remodeling.

### *baz* mutants show similar IOC defects to *Magi* mutants

We then tested whether defects in Baz membrane recruitment could be causing interrupted AJs and remodeling defects in IOCs. At 44 h APF, *baz* mutant clones (using the strong hypomorphic $baz^{815\text{-}8}$ allele) contained an excess of mislocalized IOCs (Fig. 8A′, arrowheads). Furthermore, since *baz* is required at earlier stages for correct ommatidial development, including correct morphogenesis of photoreceptors (Walther and Pichaud, 2010), many *baz* mutant ommatidia were severely disrupted; these were excluded from the subsequent analysis of AJs. In the remaining ommatidia, E-Cad-based AJs were disrupted in *baz* mutant clones at 24 h APF, similar to what was seen with *Magi* mutants. Whereas there were on average 0.72±0.16 interruptions in the cortical E-Cad staining per IOC in *baz* heterozygous tissues, this was increased to 1.26±0.30 in neighboring *baz* homozygous mutant IOCs (Fig. 8B,C). Similar results were obtained using $baz^{XI}$, an independent hypomorphic allele (0.68±0.21 interruptions per IOC in $baz^{XI}$ heterozygous, rising to 0.97±0.24 in $baz^{XI}$ homozygous; Fig. 8C).

We note that the defects in *baz* heterozygous tissue were stronger than in *Magi* or *ASPP* heterozygous tissues (where we detected ~0.25 interruptions per IOC). This might suggest that the E-Cad interruption phenotype is sensitive to the dosage of *baz*. Nevertheless, this phenotype increased in severity in *baz* homozygous tissue and was observed in two independent *baz* alleles, ruling out nonspecific genetic background effects. Finally, the defects in IOC numbers and in AJ interruptions observed in *baz* mutant tissues were not due to defects in Magi localization, as Magi was localized normally at the AJ in *baz* mutant clones (Fig. 8D). These observations support a model whereby abnormal and interrupted E-Cad/AJs in *Magi* mutant IOCs are partly due to a failure in Baz recruitment.

## DISCUSSION

As Magi is the sole *Drosophila* homolog of the three vertebrate MAGI scaffolds, it offers a powerful system with which to investigate the functions of these important proteins. Using newly generated null alleles, we have shown that Magi coordinates the number and packing of IOCs in the developing *Drosophila* pupal eye by regulating AJ dynamics. Magi is necessary in the IOCs to localize the RASSF8-ASPP complex correctly during their junctional remodeling. This ensures the integrity of E-Cad-based junctions and the correct localization of Baz, α- and β-catenin. Based on these observations and on the growing evidence of a role for Baz in AJ remodeling (Desai et al., 2013; McGill et al., 2009;

Development (2015) 142, 1-11 doi:10.1242/dev.116277

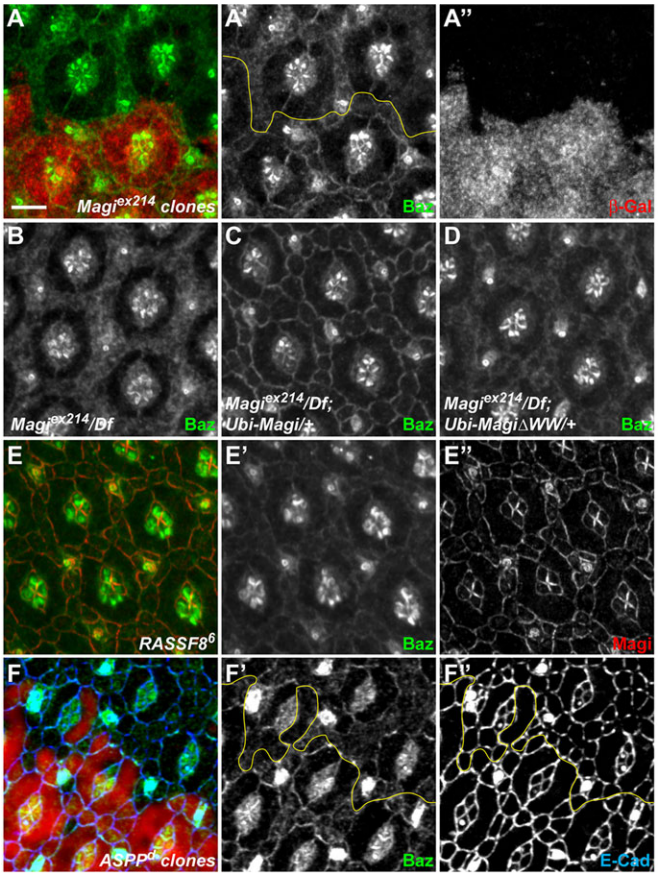


**Fig. 7. Magi is required for Baz recruitment.** (A-F″) 24-h APF pupal eye discs in different mutant backgrounds. The yellow lines (A′,F′,F″) mark the boundaries between wild-type and mutant tissues. (A-A″) In *Magi* mutant clones marked by the absence of β-galactosidase (red, A″), Baz (green, A′) is less cortical and accumulates in the cytoplasm. (B-D) In a whole *Magi* mutant background, Baz (white) is absent from the membrane in IOCs (B). Whereas cortical Baz localization is completely rescued by providing a *Magi* transgene (C), only very faint cortical recruitment of Baz could be observed with a mutant *MagiΔWW* transgene. (E-E″) In whole *RASSF8* mutant discs, Baz (green, E′) is very weakly associated with the cortex, whereas Magi localization (red, E″) is unaffected. (F-F″) In *ASPP* mutant clones marked by the absence of β-galactosidase (red), Baz (green, F′) is weaker at the membrane, in particular between IOCs [Baz at membrane in *ASPP* versus wild type=0.86; $P$=0.005 (paired $t$-test)], whereas Baz localization in primary pigment cells is less affected. Membranes are highlighted by E-Cad (blue, F″). Scale bar: 5 µm.

McKinley et al., 2012; Wei et al., 2005), we propose a model whereby, during AJ remodeling in IOCs, Magi recruits the RASSF8-ASPP complex, which helps to localize Baz at the membrane and regulates the sites of E-Cad accumulation.

### Magi and AJ remodeling

Junction remodeling is a key step during morphogenesis, in which cells in a tissue change position and neighbors. For instance, in the developing pupal eye, IOCs found between ommatidia organize as a single row of cells (Cagan, 2009). During this process existing contacts are eliminated and new ones are established by remodeling E-Cad-based junctions. In *Magi* mutants, we observed rearrangement defects and some incorrect localization of IOCs. At the same time, E-Cad-based AJs were interrupted in *Magi* mutant cells. We propose that this defect in AJ remodeling leads to IOCs remaining at the wrong place in the lattice. The most parsimonious model is that the defects in AJ remodeling trigger the defects in cell numbers seen in *Magi* mutants by preventing apoptosis, although we were unable to fully substantiate this as the effect of *Magi* on apoptosis was not statistically significant. If the model is correct, it still remains unclear how disrupted junctions would lead to a failure in apoptosis. One possibility is that IOCs only receive the correct 'death signal' when they have rearranged to contact the correct cells. Thus, in *Magi* mutants, the defective AJs would lead to apoptosis failure because the IOCs did not attain their position in the 'death zone' (Monserrate and Brachmann, 2007) to receive the killing signal.

These junctional defects are reminiscent of those seen for *magi-1* mutants in the nematode *C. elegans*, in which *magi-1* loss of function enhanced the defects caused by cadherin and catenin mutations and disrupted cell migration during enclosure (Lynch et al., 2012). MAGI scaffolds are thus implicated in the fine regulation of AJs in both flies and nematodes. A similar role has been suggested for MAGI proteins in mammalian epithelial cells. In overexpression studies, human MAGI1 reduced the Src-induced invasiveness of MDCK cells and stabilized E-Cad-mediated intercellular aggregation (Kotelevets et al., 2005). By analogy, the overexpression phenotype of *Drosophila* Magi could thus be due to stronger AJs, although this remains to be experimentally tested. The overexpression effects of MAGI-1b were sensitive to PTEN and AKT activities (Kotelevets et al., 2005) and mammalian MAGI scaffolds have also been implicated in PTEN activation through their direct binding to PTEN (Kotelevets et al., 2005; Subauste et al., 2005; Wu et al., 2000a,b; Zmajkovicova et al., 2013). However, we did not detect any physical interaction between *Drosophila* Magi and Pten, and the overexpression phenotype of Magi, at least in the *Drosophila* eye, appeared insensitive to Pten (supplementary material Table S3). Although these are negative observations, they suggest that in *Drosophila* Magi and Pten do not form a complex to regulate AJs.

Despite its effects on eye development, *Magi* mutants exhibit slightly enlarged wings. Whether this is dependent on E-Cad belt integrity and AJ dynamics remains to be established. The fact that *ASPP* shows a very similar wing phenotype supports this model (Langton et al., 2007).

### Baz membrane recruitment

Rather than binding and modulating the activity of Pten, our analysis supports a model whereby Magi, by binding to the RASSF8-ASPP complex, recruits and stabilizes Baz at the membrane. Accumulation of Baz has been shown to specify and initiate the formation of new AJs both in cellularizing embryos and in photoreceptors (McGill et al., 2009; McKinley et al., 2012; Walther and Pichaud, 2010). We propose that Baz recruited at the membrane of IOCs will in turn promote the stabilization or the proper distribution around the cell cortex of AJ material. Since biochemical and genetic experiments suggest that RASSF8 and Magi act together in a complex, we propose that the effects of Magi on AJs and on Baz membrane recruitment are mediated by RASSF8, and are thus likely to involve ASPP. Indeed, mammalian ASPP2 binds PAR3 (Cong et al., 2010; Hauri et al., 2013; Sottocornola et al., 2010) and is required for PAR3 localization at junctions both in cell culture and in the mouse neuroepithelium. This suggests that Magi might control Baz localization through ASPP. However, Baz membrane recruitment is unlikely to be the only step to form correct AJs downstream of Magi/RASSF8/ASPP. Previous studies have implicated C-terminal Src kinase (Csk) and its action on Src kinase (Langton et al., 2007, 2009), and the

Development (2015) 142, 1-11 doi:10.1242/dev.116277

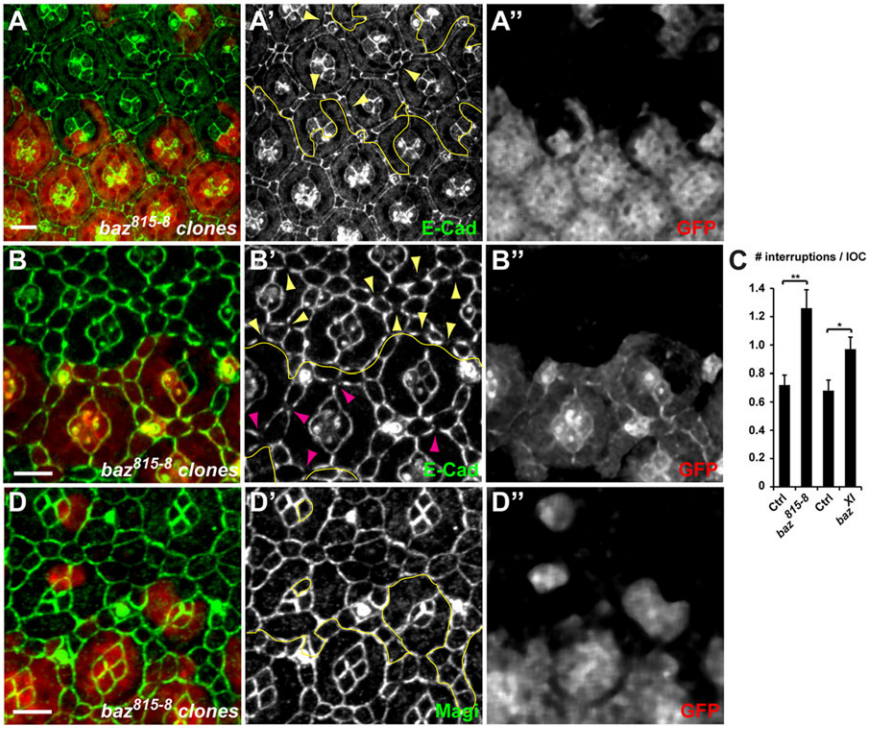


**Fig. 8. Baz controls IOC remodeling.** *baz* mutant clones are marked by the absence of GFP (red, A″,B″,D″). Yellow lines (A′,B′,D′) mark the boundaries between wild-type and mutant tissues. (A-A″) 44-h APF pupal eye discs stained for E-Cad (green, A′). In the *baz* mutant, supernumerary mislocalized IOCs are present (arrowheads). (B-B″) 24-h APF pupal eye discs. In *baz* mutant tissue, E-Cad staining (green, B′) is frequently interrupted (yellow arrowheads) compared with *baz* heterozygous tissue (purple arrowheads). (C) Quantification of E-Cad interruptions, as shown in B, in control and in two independent *baz* mutant tissues. s.e.m. is shown; ***P*=0.009, **P*=0.021 (paired *t*-test). (D-D″) 24-h APF pupal eye discs. In *baz* mutant tissue, Magi (green, D′) is found at the cortex, similarly to wild type. Scale bars: 5 µm.

relationships between Magi, Baz and Csk should be investigated in the future.

### Magi membrane localization

During IOC remodeling, Magi therefore appears to be a crucial upstream regulator of AJs. However, the mechanisms governing Magi membrane localization are still unknown. One hypothesis is that the membrane recruitments of different AJ components and regulators are dependent on each other in stabilization loops. However, this is unlikely to be the case for Magi as it is still perfectly localized at the membrane in *ASPP*, *RASSF8* and *baz* mutants, and in *ASPP; RASSF8* double mutants.

Another possibility is that Magi would require mature AJs with E-Cad to be at the membrane. We found, however, no direct correlation between E-Cad accumulation around the apical membrane and Magi membrane localization. For instance, in *ASPP; RASSF8* double-mutant cells, we could detect E-Cad belt interruptions either without (Fig. 5E, purple arrowhead) or with (Fig. 5E, yellow arrowhead) Magi, indicating that Magi localization does not require E-Cad directly. Furthermore, an extensive domain mapping of Magi failed to identify a single domain (WW or PDZ) that would be required for Magi recruitment (our unpublished observations), suggesting that it might be independent of these domains or that several redundant mechanisms may be at play. The nature of the signal required for Magi membrane localization thus remains to be uncovered.

### A MAGI-ASPP complex in mammals

Even though Magi binds to RASSF8 directly and both proteins function together during *Drosophila* eye morphogenesis, their mutant phenotypes are not identical. First, *RASSF8* mutants have a wing rounding phenotype (Langton et al., 2009), which is absent in *Magi* mutants. Second, whereas *RASSF8* has a significant role in the global developmental apoptosis rate in the pupal eye (Langton et al., 2009), no significant effect could be detected for *Magi* and *ASPP* (Langton et al., 2007). Taken together, this suggests that the assembly of a Magi-RASSF8-ASPP complex might be context dependent or that RASSF8 has Magi-independent functions.

Although the human N-terminal RASSF (RASSF7-10) proteins lack any PPxY motifs, one is present in ASPP2 and has been shown to bind to MAGI1 (Pirozzi et al., 1997). It is therefore possible that MAGI-ASPP complexes are formed in all organisms but the precise mode of interaction differs: mediated by RASSF8 in the fly, but direct in humans.

MAGI scaffolds have been suggested to play a role in tumorigenesis. First, they are bound and inactivated by several viral oncoproteins (Glaunsinger et al., 2000; Thomas et al., 2002). Second, MAGI1 has been shown to exhibit tumor suppressor activity in colorectal cancer cell lines in xenograft models (Zaric et al., 2012). Finally, mutations in *MAGI2* and *MAGI3* are reported in colon, prostate and breast cancers. Documented alterations include deletion of the second WW motif of MAGI2 (Pleasance et al., 2010), inversion of *MAGI2* (Berger et al., 2011) and a *MAGI3:AKT3* fusion leading to a disruption of *MAGI3* (Banerji et al., 2012). Based on our work, we propose that these are loss-of-function mutations. It would be interesting to investigate whether changes in AJ dynamics are associated with these MAGI mutations in human cancers and whether they contribute to tumorigenesis.

## MATERIALS AND METHODS

### *Drosophila* genetics

The viable $Magi^{ex214}$ null allele was generated by imprecise excision of the P element *P{GSV3}GS6093*. The *Magi* null phenotype is obtained either as $Magi^{ex214}$ homozygous or by crossing $Magi^{ex214}$ with the *Df(2R)Exel6072* spanning the *Magi* locus. The full-length Magi coding sequence, or Magi lacking the WW domains (MagiΔWW, removing amino acids 292-372), was amplified by PCR from cDNA LD27118 [Drosophila Genomics Resource Center (DGRC), University of Indiana, Bloomington, IN, USA] and cloned either in the pKC26w-pUbiq rescue plasmid that allows expression of the cloned fragments under the ubiquitous ubiquitin-63E promoter (see supplementary Materials and Methods for construction of the pKC26w-pUbiq rescue plasmid) or in frame with an N-terminal GFP in the pUASt vector for overexpression

Development (2015) 142, 1-11 doi:10.1242/dev.116277

studies. All transgenes (pKC26w-pUbiq and pUASt) were inserted at the same chromosomal location (86F8) using phiC31-mediated integration on the M{3xP3-RFP.attP}ZH-86Fb landing platform.

Overexpression studies were performed using *GMR-Gal4* (all cells in the differentiating eye) or *patched[559.1]-Gal4* (stripe in the wing disc) to drive expression of the UASt GFP:Magi, UASt GFP:MagiΔWW, UASt RASSF8 (Langton et al., 2009) and UASt ASPP (Langton et al., 2007) transgenes.

Genetic interactions were performed at 25°C driving *UASt GFP:Magi* under the control of *GMR-Gal4* and crossed to flies carrying mutations or overexpression UASt transgenes for the different genes of interest (see supplementary material Table S3 for list and origin).

Mutant clones were generated at high frequency in the wing using *abxUbxFLPase* or in the eye using *eyFLPase* in combination with *FRT42D Magi*$^{ex214}$, *FRT42D ASPP*$^{d}$, *FRT82B RASSF8*$^{6}$, *FRT9-2 baz*$^{815-8}$ or *FRT9-2 baz*$^{XI}$.

### Plasmids for cell culture

RASSF8 and ASPP plasmids have been described before (Langton et al., 2009). All expression plasmids were generated with the Gateway system (Invitrogen). Destination vectors are from the *Drosophila* Gateway vector collection (http://emb.carnegiescience.edu/labs/murphy/Gateway%20vectors.html). The *Magi* ORF was amplified from the LD27118 cDNA by PCR and cloned into pDONR/Zeo (Invitrogen). The point mutations in *RASSF8* and *Magi* were introduced in Entry vectors by mutagenesis PCR using PfuTurbo (Agilent). Mutations are TAT→GCT for RASSF8-Y297A, CCC→GCC for Magi-P323A, and CCA→GCA for Magi-P370A. *MagiΔWW* was subcloned using *pUASt MagiΔWW* as template (see above).

### Yeast two-hybrid screen

The RASSF8 yeast two-hybrid screen was performed by Hybrigenics (Paris, France). Full-length RASSF8 was cloned as an N-terminal LexA fusion in pB29 and used as a bait against a *Drosophila* whole embryo (0-24 h) cDNA library (RP2) in 100 mM 3-amino-triazole. $2.45\times10^{7}$ clones were screened, from which 380 positive clones were recovered and retested under the same conditions as the screen.

### Western blotting and immunoprecipitation

All immunoprecipitations were performed using lysates from S2 cells grown in Schneider's *Drosophila* medium (Gibco) supplemented with 10% FCS (Sigma-Aldrich), 100 units/ml penicillin and 100 µg/ml streptomycin. $3\times10^{6}$ S2 cells were transfected using Effectene (Qiagen). 72 h after transfection, S2 cells were lysed with HEPES lysis buffer (50 mM HEPES-NaOH pH 7.5, 150 mM NaCl, 0.5% Triton X-100) supplemented with 1 mM DTT and Complete Protease Inhibitor Cocktail (Roche). Half of the lysate was incubated with anti-FLAG M2 beads (Sigma-Aldrich) for 1 h at 4°C. The beads were washed with HEPES lysis buffer four times for 2 min each. Proteins were visualized by immunoblotting using rabbit anti-Myc (sc-789, Santa Cruz; 1:5000), rat anti-HA (3F10, Roche; 1:2000), mouse anti-FLAG (F1804, Sigma-Aldrich; 1:5000) and mouse anti-tubulin (DM1A, Sigma-Aldrich; 1:10,000) antibodies.

### Immunocytochemistry

Antibody staining of wing imaginal discs or pupal eyes were performed using standard protocols (see supplementary Materials and Methods for a full list of the antibodies used). Images were acquired with a Leica SP2-405 or a Zeiss LSM780 confocal microscope and processed using Adobe Photoshop or ImageJ (NIH).

#### Acknowledgements

We thank Michael Wehr and Paulo Ribeiro for the pKC26-pUbiq plasmid and Magi Entry clone; Florence Frayssinoux for help with directed two-hybrid tests; Elodie Forest, Lisa Héron-Milhavet and Rémi Logeay for help with 'blind' quantifications; Daniel St Johnston and Andreas Wodarz for sharing flies and antibodies; and the Bloomington Stock Center, the DGRC Kyoto Stock Center and the Developmental Studies Hybridoma Bank for flies and antibodies.

#### Competing interests

The authors declare no competing or financial interests.

#### Author contributions

Conceived experiments: S.J.B., N.T. and A.D. Performed experiments: S.Z., Y.Z. and A.D. Analyzed the data: S.Z., Y.Z., N.T. and A.D. Wrote the manuscript: S.Z., S.J.B., N.T. and A.D.

#### Funding

This work was supported by an Atip/Avenir grant to A.D.; a Wellcome Trust project grant to A.D. and S.J.B. [WT083576MA]; and a Medical Research Council programme grant to S.J.B. [G0800034]. Y.Z. acknowledges support from the Boehringer Ingelheim Fonds and Cancer Research UK (CRUK). The N.T. lab is supported by CRUK. Deposited in PMC for release after 6 months.

#### Supplementary material

Supplementary material available online at
http://dev.biologists.org/lookup/suppl/doi:10.1242/dev.116277/-/DC1

#### References

**Banerji, S., Cibulskis, K., Rangel-Escareno, C., Brown, K. K., Carter, S. L., Frederick, A. M., Lawrence, M. S., Sivachenko, A. Y., Sougnez, C., Zou, L. et al.** (2012). Sequence analysis of mutations and translocations across breast cancer subtypes. *Nature* **486**, 405-409.

**Bao, S. and Cagan, R.** (2005). Preferential adhesion mediated by Hibris and Roughest regulates morphogenesis and patterning in the Drosophila eye. *Dev. Cell* **8**, 925-935.

**Bao, S., Fischbach, K.-F., Corbin, V. and Cagan, R. L.** (2010). Preferential adhesion maintains separation of ommatidia in the Drosophila eye. *Dev. Biol.* **344**, 948-956.

**Berger, M. F., Lawrence, M. S., Demichelis, F., Drier, Y., Cibulskis, K., Sivachenko, A. Y., Sboner, A., Esgueva, R., Pflueger, D., Sougnez, C. et al.** (2011). The genomic complexity of primary human prostate cancer. *Nature* **470**, 214-220.

**Cagan, R.** (2009). Principles of Drosophila eye differentiation. *Curr. Top. Dev. Biol.* **89**, 115-135.

**Cong, W., Hirose, T., Harita, Y., Yamashita, A., Mizuno, K., Hirano, H. and Ohno, S.** (2010). ASPP2 regulates epithelial cell polarity through the PAR complex. *Curr. Biol.* **20**, 1408-1414.

**Desai, R., Sarpal, R., Ishiyama, N., Pellikka, M., Ikura, M. and Tepass, U.** (2013). Monomeric α-catenin links cadherin to the actin cytoskeleton. *Nat. Cell Biol.* **15**, 261-273.

**Dobrosotskaya, I. Y. and James, G. L.** (2000). MAGI-1 interacts with beta-catenin and is associated with cell-cell adhesion structures. *Biochem. Biophys. Res. Commun.* **270**, 903-909.

**Glaunsinger, B. A., Lee, S. S., Thomas, M., Banks, L. and Javier, R.** (2000). Interactions of the PDZ-protein MAGI-1 with adenovirus E4-ORF1 and high-risk papillomavirus E6 oncoproteins. *Oncogene* **19**, 5270-5280.

**Hauri, S., Wepf, A., van Drogen, A., Varjosalo, M., Tapon, N., Aebersold, R. and Gstaiger, M.** (2013). Interaction proteome of human Hippo signaling: modular control of the co-activator YAP1. *Mol. Syst. Biol.* **9**, 713.

**Heisenberg, C.-P. and Bellaïche, Y.** (2013). Forces in tissue morphogenesis and patterning. *Cell* **153**, 948-962.

**Ide, N., Hata, Y., Nishioka, H., Hirao, K., Yao, I., Deguchi, M., Mizoguchi, A., Nishimori, H., Tokino, T., Nakamura, Y. et al.** (1999). Localization of membrane-associated guanylate kinase (MAGI)-1/BAI-associated protein (BAP) 1 at tight junctions of epithelial cells. *Oncogene* **18**, 7810-7815.

**Kawajiri, A., Itoh, N., Fukata, M., Nakagawa, M., Yamaga, M., Iwamatsu, A. and Kaibuchi, K.** (2000). Identification of a novel beta-catenin-interacting protein. *Biochem. Biophys. Res. Commun.* **273**, 712-717.

**Kotelevets, L., van Hengel, J., Bruyneel, E., Mareel, M., van Roy, F. and Chastre, E.** (2005). Implication of the MAGI-1b/PTEN signalosome in stabilization of adherens junctions and suppression of invasiveness. *FASEB J.* **19**, 115-117.

**Langton, P. F., Colombani, J., Aerne, B. L. and Tapon, N.** (2007). Drosophila ASPP regulates C-terminal Src kinase activity. *Dev. Cell* **13**, 773-782.

**Langton, P. F., Colombani, J., Chan, E. H. Y., Wepf, A., Gstaiger, M. and Tapon, N.** (2009). The dASPP-dRASSF8 complex regulates cell-cell adhesion during Drosophila retinal morphogenesis. *Curr. Biol.* **19**, 1969-1978.

**Levayer, R., Pelissier-Monier, A. and Lecuit, T.** (2011). Spatial regulation of Dia and Myosin-II by RhoGEF2 controls initiation of E-cadherin endocytosis during epithelial morphogenesis. *Nat. Cell Biol.* **13**, 529-540.

**Lynch, A. M., Grana, T., Cox-Paulson, E., Couthier, A., Cameron, M., Chin-Sang, I., Pettitt, J. and Hardin, J.** (2012). A genome-wide functional screen shows MAGI-1 is an L1CAM-dependent stabilizer of apical junctions in C. elegans. *Curr. Biol.* **22**, 1891-1899.

**McGill, M. A., McKinley, R. F. A. and Harris, T. J. C.** (2009). Independent cadherin-catenin and Bazooka clusters interact to assemble adherens junctions. *J. Cell Biol.* **185**, 787-796.

**McKinley, R. F. A., Yu, C. G. and Harris, T. J. C.** (2012). Assembly of Bazooka polarity landmarks through a multifaceted membrane-association mechanism. *J. Cell Sci.* **125**, 1177-1190.

Development (2015) 142, 1-11 doi:10.1242/dev.116277

**Monserrate, J. P. and Brachmann, C. B.** (2007). Identification of the death zone: a spatially restricted region for programmed cell death that sculpts the fly eye. *Cell Death Differ.* **14**, 209-217.

**Pirozzi, G., McConnell, S. J., Uveges, A. J., Carter, J. M., Sparks, A. B., Kay, B. K. and Fowlkes, D. M.** (1997). Identification of novel human WW domain-containing proteins by cloning of ligand targets. *J. Biol. Chem.* **272**, 14611-14616.

**Pleasance, E. D., Cheetham, R. K., Stephens, P. J., McBride, D. J., Humphray, S. J., Greenman, C. D., Varela, I., Lin, M.-L., Ordóñez, G. R., Bignell, G. R. et al.** (2010). A comprehensive catalogue of somatic mutations from a human cancer genome. *Nature* **463**, 191-196.

**Rauzi, M., Lenne, P.-F. and Lecuit, T.** (2010). Planar polarized actomyosin contractile flows control epithelial junction remodelling. *Nature* **468**, 1110-1114.

**Reiter, C., Schimansky, T., Nie, Z. and Fischbach, K. F.** (1996). Reorganization of membrane contacts prior to apoptosis in the Drosophila retina: the role of the IrreC-rst protein. *Development* **122**, 1931-1940.

**Sakurai, A., Fukuhara, S., Yamagishi, A., Sako, K., Kamioka, Y., Masuda, M., Nakaoka, Y. and Mochizuki, N.** (2006). MAGI-1 is required for Rap1 activation upon cell-cell contact and for enhancement of vascular endothelial cadherin-mediated cell adhesion. *Mol. Biol. Cell* **17**, 966-976.

**Sottocornola, R., Royer, C., Vives, V., Tordella, L., Zhong, S., Wang, Y., Ratnayaka, I., Shipman, M., Cheung, A., Gaston-Massuet, C. et al.** (2010). ASPP2 binds Par-3 and controls the polarity and proliferation of neural progenitors during CNS development. *Dev. Cell* **19**, 126-137.

**Subauste, M. C., Nalbant, P., Adamson, E. D. and Hahn, K. M.** (2005). Vinculin controls PTEN protein level by maintaining the interaction of the adherens junction protein beta-catenin with the scaffolding protein MAGI-2. *J. Biol. Chem.* **280**, 5676-5681.

**Tepass, U. and Harris, K. P.** (2007). Adherens junctions in Drosophila retinal morphogenesis. *Trends Cell Biol.* **17**, 26-35.

**Thomas, M., Laura, R., Hepner, K., Guccione, E., Sawyers, C., Lasky, L. and Banks, L.** (2002). Oncogenic human papillomavirus E6 proteins target the MAGI-2 and MAGI-3 proteins for degradation. *Oncogene* **21**, 5088-5096.

**Vidal, M., Larson, D. E. and Cagan, R. L.** (2006). Csk-deficient boundary cells are eliminated from normal Drosophila epithelia by exclusion, migration, and apoptosis. *Dev. Cell* **10**, 33-44.

**Walther, R. F. and Pichaud, F.** (2010). Crumbs/DaPKC-dependent apical exclusion of Bazooka promotes photoreceptor polarity remodeling. *Curr. Biol.* **20**, 1065-1074.

**Wei, S.-Y., Escudero, L. M., Yu, F., Chang, L.-H., Chen, L.-Y., Ho, Y.-H., Lin, C.-M., Chou, C.-S., Chia, W., Modolell, J. et al.** (2005). Echinoid is a component of adherens junctions that cooperates with DE-Cadherin to mediate cell adhesion. *Dev. Cell* **8**, 493-504.

**Wu, X., Hepner, K., Castelino-Prabhu, S., Do, D., Kaye, M. B., Yuan, X.-J., Wood, J., Ross, C., Sawyers, C. L. and Whang, Y. E.** (2000a). Evidence for regulation of the PTEN tumor suppressor by a membrane-localized multi-PDZ domain containing scaffold protein MAGI-2. *Proc. Natl. Acad. Sci. USA* **97**, 4233-4238.

**Wu, Y., Dowbenko, D., Spencer, S., Laura, R., Lee, J., Gu, Q. and Lasky, L. A.** (2000b). Interaction of the tumor suppressor PTEN/MMAC with a PDZ domain of MAGI3, a novel membrane-associated guanylate kinase. *J. Biol. Chem.* **275**, 21477-21485.

**Zaric, J., Joseph, J.-M., Tercier, S., Sengstag, T., Ponsonnet, L., Delorenzi, M. and Rüegg, C.** (2012). Identification of MAGI1 as a tumor-suppressor protein induced by cyclooxygenase-2 inhibitors in colorectal cancer cells. *Oncogene* **31**, 48-59.

**Zmajkovicova, K., Jesenberger, V., Catalanotti, F., Baumgartner, C., Reyes, G. and Baccarini, M.** (2013). MEK1 is required for PTEN membrane recruitment, AKT regulation, and the maintenance of peripheral tolerance. *Mol. Cell* **50**, 43-55.

# SUPPLEMENTARY MATERIAL

## SUPPLEMENTARY MATERIALS & METHODS

### *Construction of the pKC26w-pUbiq rescue plasmid*

pKC26w-pUbiq was generated from pKC26-pUbiq and pW25. First, to obtain pKC26-pUbiq, pKC26 was digested with PstI and XbaI (to remove the 10X UAS sequence) and a new MCS was introduced. The *ubiquitin-63E* promoter was cloned into MluI and KpnI sites. Subsequently, to allow insertion into any landing site, the full mini-white gene was restored. This was done by subcloning the missing mini-white gene from pW25 and mutagenizing an internal DraIII site within mini-white to allow for insertion into DraIII and SpeI sites of pKC26-pUbiq.

### *Immunocytochemistry*

Primary antibodies used were: guinea pig anti-Magi (polyclonal directed against Magi aa 790-1202 generated for this study; 1:2000), rat anti-ASPP (1:500) (Langton et al., 2007), rabbit anti-RASSF8 (1:500) (Langton et al., 2009), rabbit anti-Bazooka (1:500) (gift from A. Wodarz; (Wodarz et al., 1999), rat anti-E-Cad (DCAD2, Developmental Studies Hybridoma Bank – DSHB; 1:25), mouse anti-Arm (N2 7A1, DSHB; 1:25), rat anti-α-Catenin (DCAT-1, DSHB; 1:25), mouse anti-β-Galactosidase (DSHB 40-1a; 1:25), mouse anti-Dlg (4F3, DSHB; 1:25), rabbit anti-aPKC (anti-PKCz C-20, SantaCruz; 1:500), rabbit anti-GFP (A6455, Molecular Probes; 1:2000), rabbit anti Cleaved Drosophila Dcp-1 (9578, Cell Signaling; 1:200).

### *Quantifications*

*Quantification of IOCs:* the inter-ommatidial lattice is composed of 9 IOCs per ommatidium, six 2° and three 3° pigment cells. Each 2° pigment cell is shared by two

ommatidia and 3° pigment cell by three ommatidia. For quantification of IOCs per ommatidium, we selected complete ommatidial units and counted independently all IOCs surrounding them. Statistical relevance was obtained by performing unpaired two-tailed student t-test on raw data obtained from at least 5 experiments.

*Quantification of E-Cad interruptions:* 22-26h APF pupal retinas were stained with anti-E-Cad antibody. At least 7 confocal stacks spanning the entire depth of the tissues from independent retinas were taken showing mutant and wild type tissues, and flattened using the maximum projection tool in ImageJ (NIH). This ensured that no out of focus E-Cad staining was left out. Gaps in E-Cad staining were then counted in IOCs and divided by the number of IOCs to obtain the interruption per IOC index. Significance was then assessed by unpaired two-tailed student t-test.

*Quantification of Baz, α-Cat, or Arm membrane levels:* 22-26h APF pupal retinas were stained with the relevant antibodies and at least 7 retinas were imaged as indicated above. Using the "Freehand line selections" a line was drawn following IOC/IOC membrane as shown by an E-Cad staining. "Mean Gray Value" gave of average fluorescence intensity along the lines. At least 15 IOC/IOC membranes were quantified this way per stack and per territory (wild type (wt) vs mutant). Average fluorescence intensity for IOC/IOC membranes per image were then obtained showing substantial differences between images highlighting the importance of the clonal analysis. When levels were compared between wt and mutant tissues from the same image, and thus stained, treated, and imaged exactly the same way, membrane levels were always higher in wt. Statistical relevance was then assessed by paired two tailed student t-test using the wt/mutant tissues pairs.

## SUPPLEMENTARY REFERENCES

Langton, P. F., Colombani, J., Aerne, B. L. and Tapon, N. (2007). Drosophila ASPP regulates C-terminal Src kinase activity. *Dev. Cell* 13, 773–782.

Langton, P. F., Colombani, J., Chan, E. H. Y., Wepf, A., Gstaiger, M. and Tapon, N. (2009). The dASPP-dRASSF8 complex regulates cell-cell adhesion during Drosophila retinal morphogenesis. *Curr. Biol. CB* 19, 1969–1978.

Wodarz, A., Ramrath, A., Kuchinke, U. and Knust, E. (1999). Bazooka provides an apical cue for Inscuteable localization in Drosophila neuroblasts. *Nature* 402, 544–547.

## SUPPLEMENTARY FIGURES

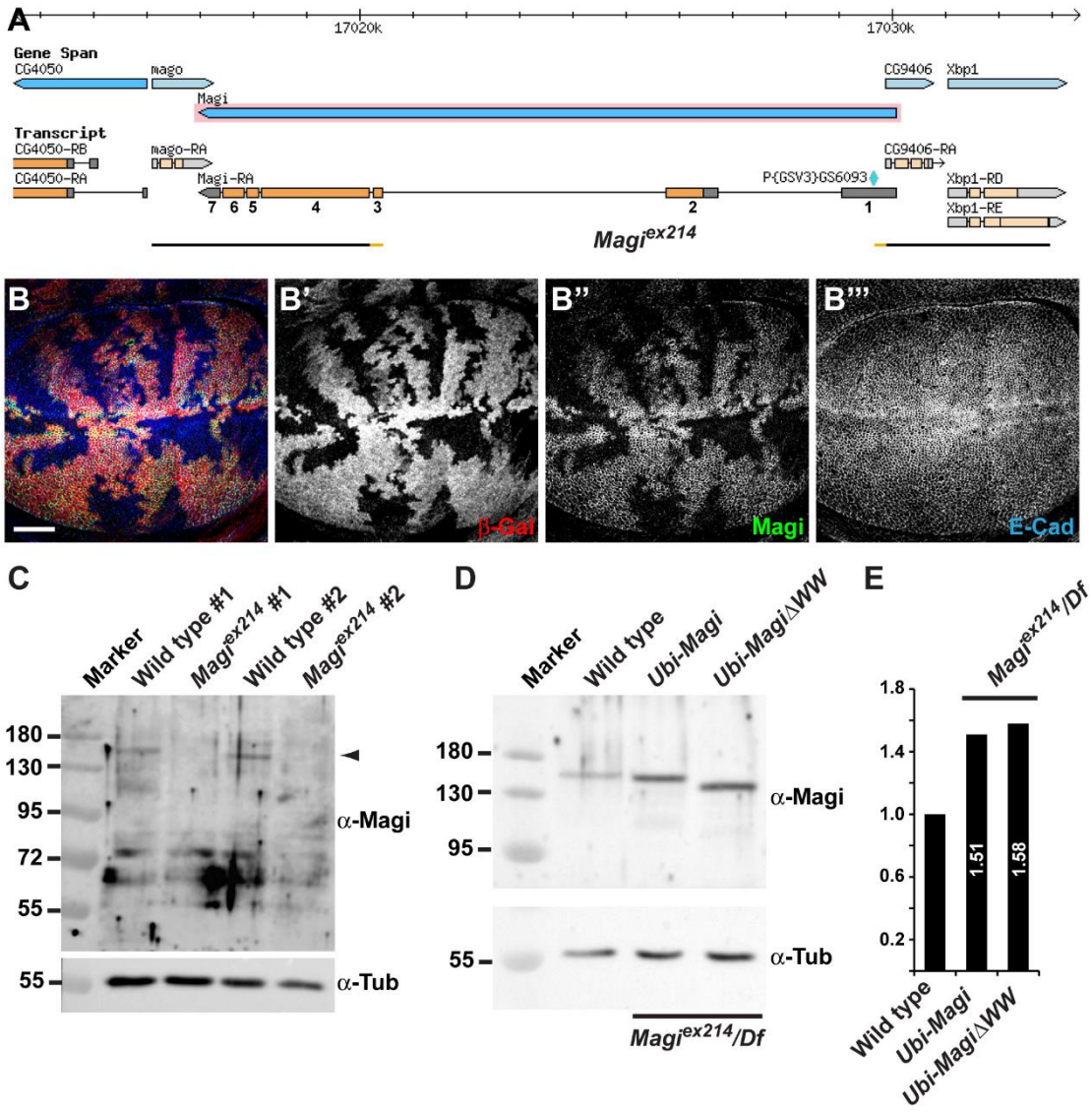


**Figure S1. *Magi* expression levels.**

**A.** *Magi* locus (adapted from Flybase GBrowse) showing novel *Magi* allele. The *Magi*$^{ex214}$ local deletion was generated by mobilizing the viable GS6093 P element (green diamond) and mapped by PCR (absent DNA is represented by the interrupted black line; orange segments indicate regions of uncertainty). The *Magi* transcript is represented by shaded boxes (orange, coding; grey, non coding), and numbers indicate position of exons used in the text.

**B.** *Magi*$^{ex214}$ mutant clones in the larval wing disc, marked by the absence of β-Galactosidase (red; B'). In mutant cells, Magi protein is totally absent (green; B"), while E-Cadherin (E-Cad; blue; B"') is unaffected. Bar, 25μm.

**C.** Western blot characterization of the *Magi*$^{ex214}$ allele. Top panel: Western blot analysis using the anti-Magi antibody (α-Magi) of total protein extracts from two independent experiments (#1-2) from isolated pupal eye discs at 22-26h APF either from wild type controls or from *Magi*$^{ex214}$ homozygotes. A band migrating slightly above 130kDa and corresponding to the predicted size for the Magi protein is present in controls but disappears in *Magi*$^{ex214}$ mutants. An increase in other bands was not observed suggesting that other Magi fragments are not translated in the *Magi*$^{ex214}$ mutants. Bottom panel: same membrane as in top but re-blotted with an anti-Tubulin antibody (α-Tub) used as a loading control.

**D.** Western blot characterization of the *Ubi-Magi* rescues. Top panel: Western blot analysis using the anti-Magi antibody (α-Magi) of total protein extracts from isolated pupal eye discs at 22-26h APF either from wild type controls or from *Magi mutants (Magi*$^{ex214}$*/Df(2R)Exel6072* trans-heterozygotes) carrying one copy of *Ubi-Magi* or *Ubi-MagiΔWW* transgenes. Bottom panel: same extracts as in top blotted with an anti-Tubulin antibody (α-Tub) used as a loading control.

**E.** Relative amounts of Magi protein from the western blot shown in B. After normalization with the Tubulin loading control, the Ubi-Magi and Ubi-MagiΔWW are expressed respectively 1.51 and 1.58 times more than the endogenous Magi protein. This shows that the Ubiquitin promoter driven Magi rescue constructs are expressed at very similar levels to the endogenous protein, and that the MagiΔWW construct is as stable as wild type Magi.

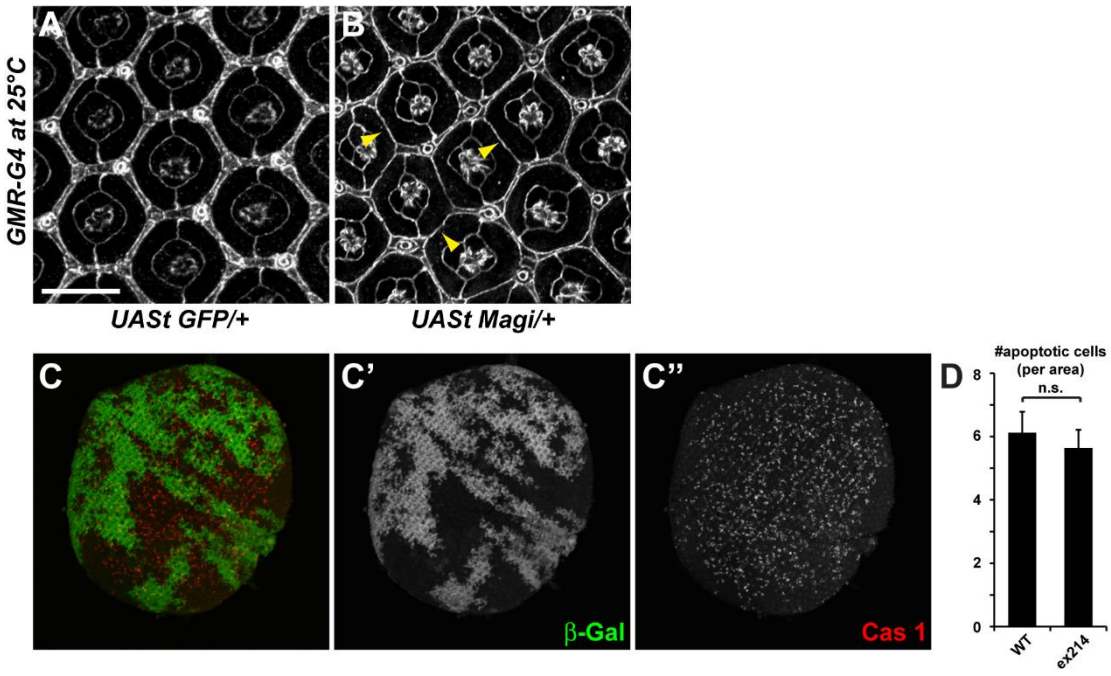


**Figure S2. *Magi* and the control of IOC cell number.**

**A-B.** Pupal eye at 44h APF stained for E-Cad (white) showing the ommatidial organization. When overexpressed under the control of the *GMR-Gal4* driver, Magi produces pupal eyes with fewer IOCs (B; yellow arrowheads) than control (A). Bar, 10 µm.

**C.** Whole pupal retina with Magi mutant homozygous clones marked by the absence of β-Galactosidase (green, C') and stained for activated Dcp1 (red, C").

**D.** Quantification of the number of activated caspase-1 puncta per arbitrary area unit in wild type (WT; β-Galactosidase positive) and Magi mutant (β-Galactosidase negative) tissues. No statistical difference was observed; sem is shown; paired two-tailed student t-test on 15 pairs of tissues; p=0.395).

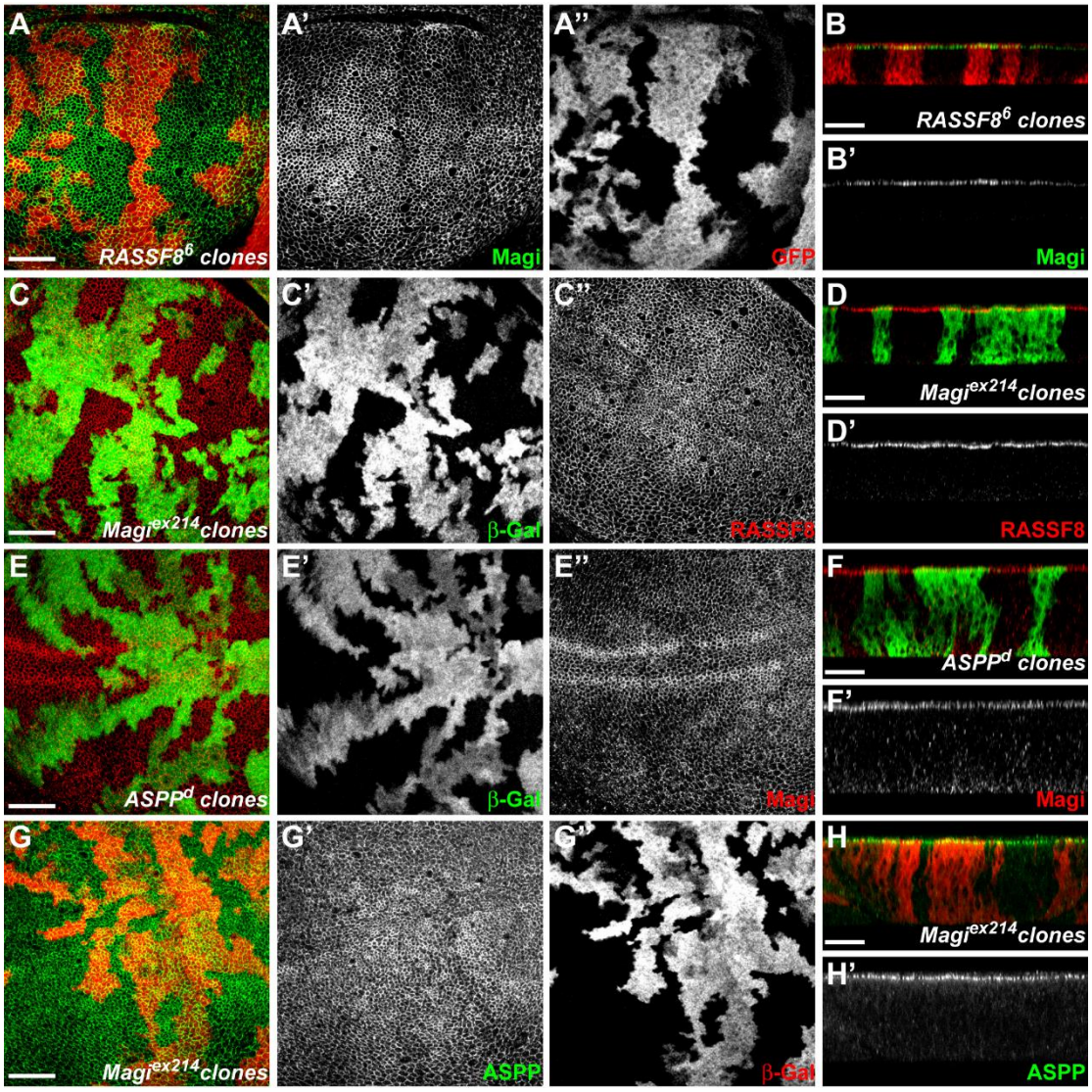


**Figure S3. In 3rd instar larval wing discs, Magi and the RASSF8/ASPP complex localize independently to AJs.**

**A-D.** Magi and RASSF8 localize independently. In *RASSF8* mutant clones (A,B), marked by the absence of GFP (red; A''), Magi protein levels and apical localization are unaffected (green; A',B'). Similarly, in *Magi* mutant clones (C,D) marked by the absence of β-Galactosidase (green; C'), RASSF8 protein levels and apical localization are unaffected (red; C''&D').

**E-H.** Magi and ASPP localize independently. In *ASPP* mutant clones (E,F), marked by the absence of β-Galactosidase (green; E'), Magi protein levels and apical

localization are unaffected (red; E"&F'). Similarly, in *Magi* mutant clones (G,H) marked by the absence of β-Galactosidase (red; G"), ASPP protein levels and apical localization are unaffected (green; G'&H').

xy apical (A,C,E,G) and z (B,D,F,H) confocal sections. Bars, 20 μm.

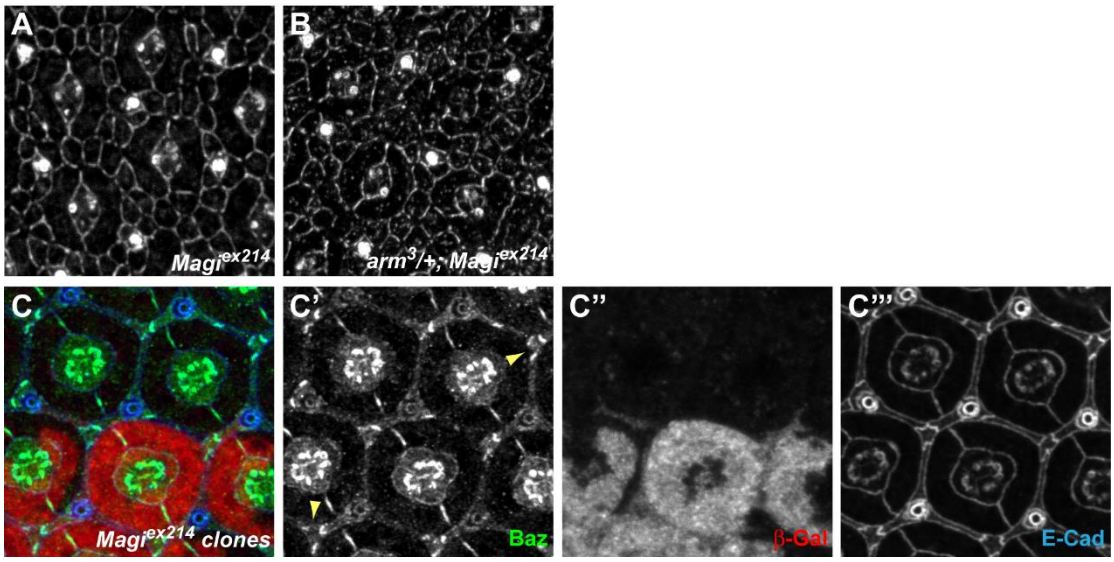


***Figure S4. Magi and AJ formation.***

**A-B.** 24h APF pupal eye discs stained for E-Cad (white; A-B). The E-Cad interruptions in *Magi*$^{ex214}$ homozygous mutants (A) is strongly enhanced by the removal of one copy of β-catenin (*arm*$^{3}$/+; B).

**C.** At 44h APF, Baz (green; C') is localized correctly at the level of inter-IOCs membranes (yellow arrowheads), both in wild type and in *Magi* mutant clones marked by the absence of β-Galactosidase (red; C''). Membranes are highlighted with E-Cad (blue; C''').

**Table S1. *Magi* mutant flies have slightly bigger wings.**

Adult female wings measurement in arbitrary units (pixels) in the indicated genotypes. *Magi* mutant wings are both slightly longer and wider than controls giving rise to wings slightly bigger but of the correct shape (ratio width / length similar to control). This phenotype is different from the round wing phenotype of *RASSF8* mutants.

**Table S2. Magi yeast 2-hybrid clones interacting with RASSF8.**

Clones corresponding to Magi fragments and isolated in a yeast 2-hybrid screen using full length RASSF8 as bait. 3 independent clones were recovered. The minimal common regions in these clones spans from nucleotide 852 to nucleotide 1134 of Magi corresponding to amino-acids 284 to 378 around the two WW domains (see Figure 2).

**Table S3. Genetic modifiers of the rough eye phenotype of overexpressed Magi.**

List of mutants tested for dosage sensitivity by scoring any modification of the external adult roughness induced by UASt Magi overexpression in the eye under the control of the *GMR-Gal4* driver at 25°C.

Columns are:

- Genotype: presenting the relevant genotype. Mutants have been grouped by pathway.
- Score: indicating the level of modification. Rescues are highlighted in green; enhancements in red.
- Origin of mutation: indicates where the described mutations can be obtained; BSC = Bloomington Stock Center.
- Note: additional information available regarding the mutation used.

**Table S1. *Magi* mutant flies have slightly bigger wings.**

| Genotype | Mean length | Stdv length | Mean width | Stdv width | Mean w/l | Stdv w/l | n |
|---|---|---|---|---|---|---|---|
| *Df(2R)6072/+* | 782.37 | 16.39 | 560.65 | 12.45 | 0.72 | 0.008 | 19 |
| *Magi[ex214]/+* | 781.35 | 19.26 | 548.60 | 10.00 | 0.70 | 0.011 | 19 |
| *Magi[ex214]/Df(2R)6072* | 810.09 | 18.07 | 601.97 | 14.61 | 0.74 | 0.015 | 18 |
| *Magi[ex214]/Magi[ex214]* | 814.62 | 11.76 | 579.60 | 10.23 | 0.71 | 0.012 | 16 |
| *RASSF8[6]/RASSF8[6]* | 789.14 | 13.21 | 654.37 | 10.07 | 0.83 | 0.012 | 19 |

**Conclusion:** *Magi* mutant wings are both longer and larger than control, but ratio width/length (w/l) is the same, ie wings are not rounder. This phenotype is different from the *RASSF8* mutant round wing phenotype.

**Table S2. Magi yeast 2-hybrid clones interacting with RASSF8.**

Y2H screen using full length RASSF8 as bait.

Only clones relative to Magi are presented here.

*Drosophila* CG5053 (1-607) vs *Drosophila* Whole Embryo RP2 (0-12+12-24)

| Clone name | Global PBS | Gene name | Start | Stop | Remarks |
|---|---|---|---|---|---|
| C-137 | A | Magi CG30388 | No Data | 1238 | Ends after the WW domains |
| C-213 | A | Magi CG30388 | 519 | 1134 | N-ter and WW domains |
| C-343 | A | Magi CG30388 | 852 | 1239 | WW domains |

Summary of PBS categories
A : Very high confidence in the interaction
B : High confidence in the interaction
C : Good confidence in the interaction
D : Moderate confidence in the interaction
E : Interactions involving highly connected prey domains, warning of non-specific interaction
F : Experimentally proven technical artifacts
N/A : The PBS is a score that is automatically computed through algorithms and cannot be attributed

**Table S3. Genetic modifiers of the rough eye phenotype of overexpressed Magi.**

| Genotype | Score | Origin | notes |
|---|---|---|---|
| **PTEN** | | | |
| *FRT40A pten[DS189]/+* | none | D. St Johnston | |
| *FRT40A pten[C494]/+* | none | D. St Johnston | |
| *Df(2L)ED729/+* | none | BSC | Deficiency for *pten* |
| *Akt[04223]/+* | none | BSC | |
| *Df(1)BSC538/+* | none | BSC | Deficiency for *Dsor1* |
| **HIPPO PATHWAY** | | | |
| *ex[1]/+* | none | N. Tapon | |
| *ex[697]/+* | none | N. Tapon | |
| *kibra[del]/+* | none | N. Tapon | |
| *FRT82B sav[3]/+* | slightly worse | N. Tapon | |
| *sav[4]/+* | none | N. Tapon | |
| *FRT82B wts[X1]/+* | none | N. Tapon | |
| *wts[M541]/+* | none | N. Tapon | |
| *yki[B5]/+* | none | N. Tapon | |
| **RASSF8/ASPP** | | | |
| *RASSF8[4]/+* | worse | N. Tapon | drives overexpression |
| *UAS-RASSF8/+* | worse | N. Tapon | drives overexpression |
| *RASSF8[6]/+* | rescue | N. Tapon | |
| *FRT82B ASPP[d]/+* | none | N. Tapon | |
| *FRT82B ASPP[8]/+* | none | N. Tapon | |
| *Csk[J1D8]/+* | none | BSC | |
| *puc[A251.1F3]/+* | none | BSC | |
| **OTHERS** | | | |
| *FRT82B pyd[tamou]/+* | none | A. Djiane | |
| *FRT82B pyd[ex147]/+* | none | A. Djiane | |
| *aPKC[k06403]/+* | none | BSC | |